



Numerical Analysis of the Thermal Management Strategies of Electric Vehicle Battery: A Review

P. Satheysh Paval¹ · T. Karthikeya Sharma¹ · Phani Kumar Mallisetty² · Balaji Chandrakanth³ · T. Srinivas Reddy⁴

Received: 30 October 2023 / Accepted: 9 January 2024 / Published online: 26 February 2024

© The Author(s) under exclusive licence to International Center for Numerical Methods in Engineering (CIMNE) 2024

Abstract

In highly fluctuating ambient conditions, the effective Thermal Management Strategies of the Battery guarantee the safe and stable operation of an electric vehicle as high-power density batteries like lithium-ion batteries (LIBs) are temperature dependent. Exceeding the thermal limits of the LIB, initially degrades the battery's performance, leading to serious problems of thermal runaway, and fire hazards. The battery thermal management system (BTMS) of the electric vehicle aids in overcoming this by thermally comforting the battery by employing various strategies based on the environmental conditions. This significance of a BTMS of EVs with the increasing concerns of reducing conventional energy and transportation systems due to environmental and efficiency issues has allowed for extremely consistent growth in the BTMS as a research field resulting in the development of many types of thermal management systems which can limit the battery's operating temperature and maintain temperature homogeneity. The present review focuses the Computational Fluid Dynamics (CFD) analysis on the thermal performance of newly developed and modified BTMS depicting the temperature fields with the pressure drop, as a function of structural and operational parameters, to the closest value of the actual experimental approach which requires high cost and consumes more time. Thereby, the numerical analysis of recently developed BTMS strategies with the obtained results and suggestions for further improvement is summarized providing a clear idea to the readers and upcoming researchers for their future research.

1 Introduction

The global concerns of environmental pollution and the energy crisis led to an efficient energy utilization of electric vehicles (EVs) as a prominent alternative to the traditional internal combustion-engine automobiles [1] as multiple renewable sources can account for the electric energy consumed by EVs. The instant torque-producing ability along with low maintenance and running costs of EVs compared to conventional vehicles [2] increased the attention towards

EVs. By 2030, 15 times more EVs than in 2017, about 18.7 million EVs are predicted to be on the roads [3].

The performance and advancement of EVs is directly influenced by the batteries which are the primary power source of EVs [3, 4]. Many companies like GM, Honda, Ford, Nissan, BMW, Tesla, and BYD etc. that hold a large pie in the EV market prefer lithium-ion battery (LIB) cells [4] due to their high efficiency with high specific energy, lack of memory effect, extended lifespan and low self-discharge rate [5–7]. The generation and accumulation of heat with the operational temperature of LIBs over the operating cycle declines the performance leading to critical safety issues, where elevated temperature causes electrolyte decomposition [8] and thermal runaway leading to an explosion of batteries [9], and extremely low temperatures suppress the energy and battery power [10, 11].

From the National Renewable Energy Laboratory (NREL), Pesaran et al. limits the operational temperature between 15 and 35 °C for optimal performance [12] whereas the theoretical temperature ranges between – 10.00 to 50.00 °C [13]. In addition, temperature homogeneity is to be maintained such that only 5 °C of maximum deviation in

✉ T. Karthikeya Sharma
tks@nitandhra.ac.in

¹ Department of Mechanical Engineering, NIT Andhra Pradesh, Tadepalligudem, India

² Electric Mobility and Tribology Research Group, CSIR-Central Mechanical Engineering Research Institute, Durgapur, India

³ Advanced Casting Research Group, CSIR-Central Mechanical Engineering Research Institute, Durgapur, India

⁴ SHAR, Indian Space Research Organization, Nellore, India

temperature between distinct battery cells of a battery pack is allowed. A quick deterioration of LIBs leading to greater risk happens on exceeding this safe zone temperature limit [14]. Therefore, the safe and reliable performance of the electric vehicle batteries are assured by the battery thermal management system (BTMS) of the vehicle that maintains the optimal and consistent distribution of temperature among the distinct cells of the battery pack.

1.1 Battery Thermal Management System

The Battery Thermal Management System of a vehicle must be a structurally lightweight compact system, easily packed and positioned in the vehicle such that readily available for maintenance purposes. On the performance basis, the capability of the thermal management system to adapt the ambient environments on lowering or increasing the battery temperature by imparting adequate cooling or heating effects is more important as stated by Pesaran [15] and adds that the system should include an effective insulation preventing the effects of abrupt spikes in temperature on the performance of battery and a proper ventilation system to exhaust the hazardous gases. In addition, the BTMS of a vehicle must consume less parasitic power to provide an acceptable temperature control as specified by the battery manufacturer.

The control of heat generation and accumulation in the battery pack during the charging and discharging cycles are a crucial concern for the BTMS as they are the prime factors for spiking temperature and uneven distribution of temperature [16] within the battery system resulting localized deterioration. The battery operation temperature between the range of 20 to 40 °C is preferred on considering the allowable ranges in charging and discharging cycles which are generally—20 to 60 °C, and 0 to 45 °C respectively [17]. When the battery temperature falls below its operating limit, the efficiency of the battery in delivering the energy drops due to the increase in internal resistance. On the other hand, the rate of battery degradation accelerates with the rise in internal impedance of the battery when the battery temperature exceeds the operational limit resulting in reduced performance and cycle life, and on extreme conditions of temperature may end up in thermal runaway where the energy stored in the battery releases in the form of heat, gas or even fire seriously risking the vehicle and the passengers of the vehicle. C-rate representing the discharge and charge current, measures the rapidness of the discharging/charging in a battery compared to its maximum capacity thereby the quantity of energy stored in the battery can be determined [18]. 1C rate represents a battery fully energized rated at 1 Ah delivers a current of 1 A for a time period of one hour and batteries with high C-rates are known as fast charging/discharging batteries having relatively more heat generation

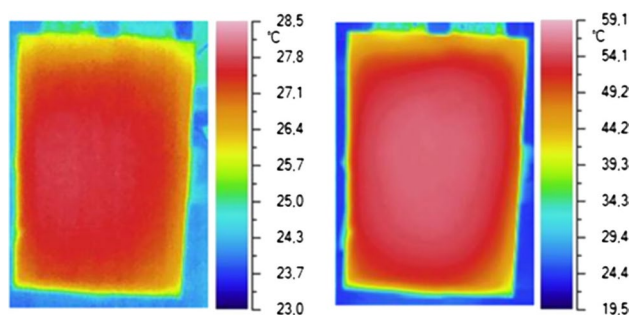


Fig. 1 Battery hot spots during discharge conditions of 1C rate and 10C rate [20]

compared with normal batteries as shown in Fig. 1 [19, 20]. In addition to this, heat generation may also be due to mixing, change of phase and different electro-chemical reactions in the cell [21, 22]. Thereby, effective stability with protection and peak performance can be achieved by the establishment of a suitable system performing an appropriate thermal management strategy which dissipates the heat generated and maintains homogeneous thermal fields by avoiding the accumulation of excess heat.

2 Classification of BTMS

Based on the three primary operating circumstances of power consumption, working fluid and arrangement, the BTMS of an electric vehicle can be categorized as by Arora [23] depicted in Fig. 2 and in addition, the thermal performance of the battery can also be affected by the modification of the electrode with surface coating, doping or etc. and even by varying the thickness of the electrode.

2.1 Power Consumption of the BTMS

An active Battery Thermal Management System (BTMS) refers to a system that includes power consuming devices, like blowers, pumps or evaporators in the cooling loop. On the hand a passive BTMS does not have any of these equipment [24]. However, in terms an active BTMS actively manages the cooling rate by turning on the power consuming equipment according to predefined settings. Additionally Thermal Management Systems absorb and remove the heat from the system with the aid of a working fluid or coolant. This heat can be absorbed either as sensible heat, which raises the temperature of the working fluid or as latent heat causing it to undergo phase transition. In general, active systems remove heat as sensible heat while passive systems remove heat as latent heat.

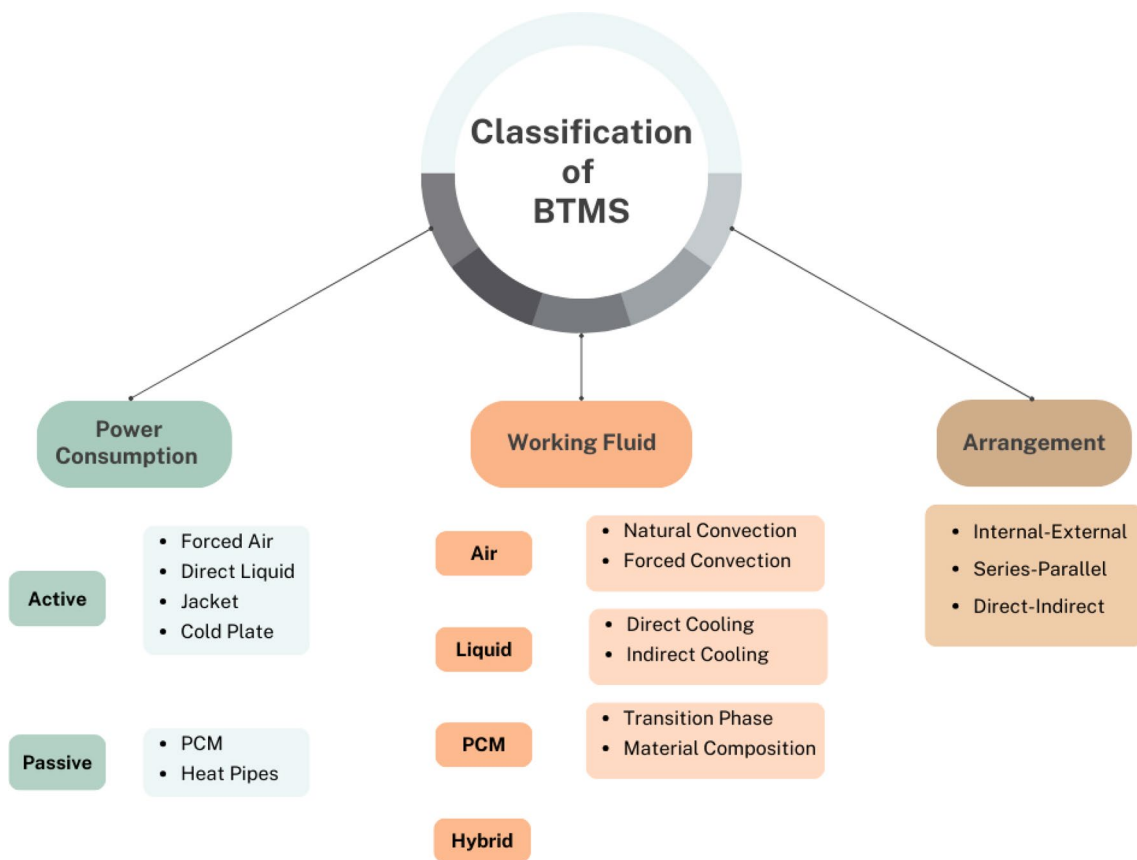


Fig. 2 Classification of various strategies of battery thermal management [23]

2.2 Working Fluid Employed as a Cooling Medium in the BTMS

According to the working fluid which absorbs the excess heat in extreme hot conditions and generates heat at low temperature conditions, the BTMS can be categorized as (Fig. 3):

2.2.1 Air Cooled BTMS

Air cooling is a technique that has been extensively studied and widely implemented in applications when there is constrained design space in the vehicle [26, 27]. Mostly, the forced air supplied by an active system like fan connected to the battery pack helps in limiting the excessive temperature rise during extreme battery discharge scenarios [28]. Another approach involves utilizing conditioned air, from the vehicles air conditioning unit [29]. To achieve cooling

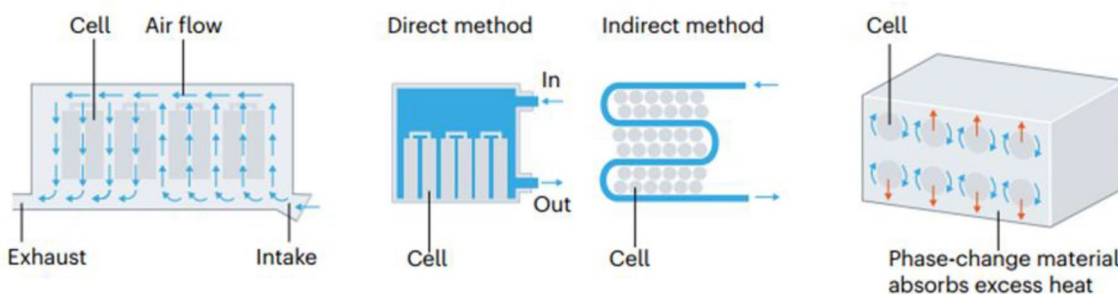


Fig. 3 Different thermal management systems [25]

in the BTMS the natural convection process is also relied, where the heat is dissipated by directing the flow of air from the external environment of a moving vehicle to the battery pack inside without any active systems. This airflow cools the BTMS by carrying away the surplus heat and releasing it into the surrounding air.

2.2.2 Liquid Cooled BTMS

Liquid cooling includes cooling in both indirect and direct manner, is a potential path for large scale EV BTMSs to overcome the constraints of air-cooling systems [30]. Indirect strategy of cooling is one of the most extensively utilized EV BTMS, using popular coolants of ethylene glycol and water in different proportion mixes. Normally, the coolant travels through channels of pipes or cooling plates, transporting the rejected heat out of the battery pack. The Tesla Model 3 employs side cooling through serpentine tubing coupled to cylindrical cells [31]. The bottom cooling system is used by the EQC of Mercedes-Benz, e-tron of Audi, and Taycan of Porsche.

A heat transfer jacket serves as a bridge between the battery cells and the liquid coolant in a standard liquid-cooling BTMS. Its efficiency in transferring heat considerably influences the system's cooling efficiency. Cooling jacket enhancements are often done by changing heat conducting materials or adjusting geometrical features (Fig. 4).

The immersion of battery in a non-conductive dielectric fluid, facilitates a direct contact of the coolant with the cell, in a process known as direct liquid cooling, sometimes known as immersion cooling. Dielectric fluids are used, including fluorinated hydrocarbons, silicone oils, and hydrocarbon oils. Among all cooling techniques, it has the superior capability to offer the finest pack and cell temperature homogeneity since direct coolant contact with the surfaces of the cell will further decrease the thermal contact resistances that are present in indirect cooling systems [32].

Another type of indirect liquid cooling, heat pipes being a passive system offers significantly higher thermal conductivities than traditional liquid cooling methods by evaporating and condensing a two-phase working fluid inside a



Fig. 4 Cooling plate used in EV (Courtesy: valeo.com)

sealed thermally conductive pipe, as shown in Fig. 5. They are referred to as thermal superconductors because their total thermal conductivity is 91 times greater than that of an equivalent-sized copper rod [33]. The device's flexible shape can fit a range of space sizes. Heat pipe is a top option for an EV battery because of these enticing properties.

2.2.3 PCM Cooled BTMS

Phase change materials (PCMs) play a role, in absorbing or releasing an amount of latent heat during the phase transition process. Enhancing the uniformity of battery temperatures involves utilizing PCMs with latent heat for phase transition along with minimal temperature and volume changes [35]. As power batteries continue to advance, a standalone PCM-based thermal management approach becomes insufficient leading to the integration of PCM with other cooling strategies for effective performance. Phase change fluids (PCFs) and solid encapsulated PCMs are incorporated as heat transfer mediums within battery packs of Li ions for efficient heat transfer. The introduction of PCMs such as PCFs and flexible phase change materials (FPCMs) has overcome the limitations associated with conventional PCM usage in battery thermal management (Fig. 6) [36, 37].

2.3 Arrangement of the Components Inside the BTMS

Based on the distribution techniques of the working fluid within the battery pack, it is classified as,

- Internal–External,
- Parallel–Series,
- Indirect–Direct.

3 Governing Equations

The standard equations expressing the thermo-hydraulic process taking place in the battery's thermal management system are,

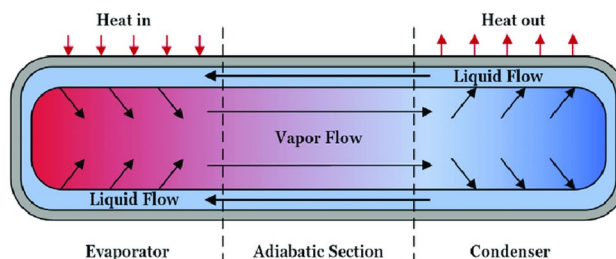


Fig. 5 Working of Heat pipe [34]

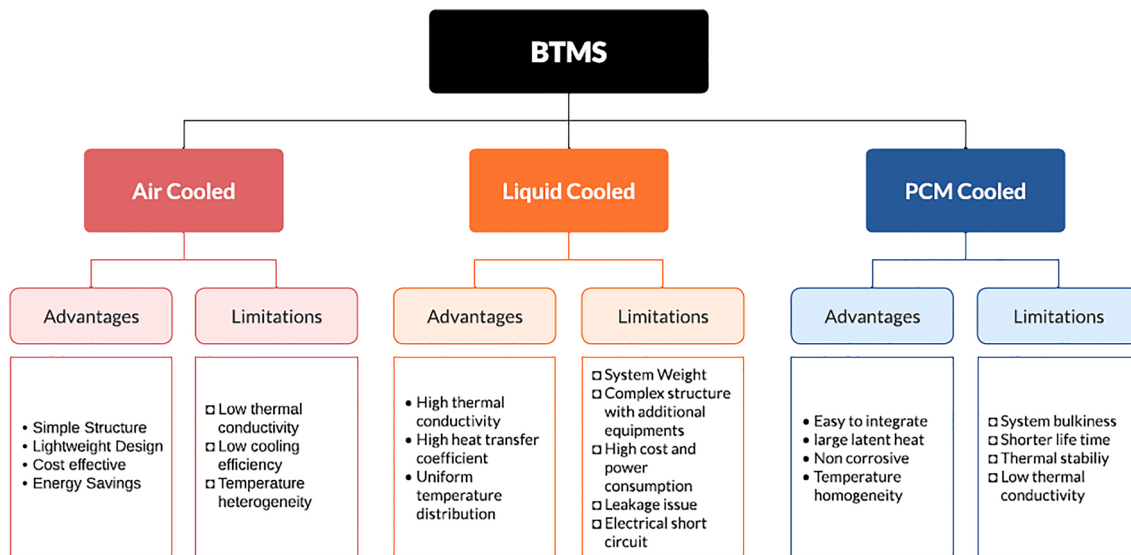


Fig. 6 Summary of the advantages and limitations of BTMS

Continuity equation, $\frac{\partial \rho_f}{\partial t} + \nabla \cdot (\rho_f \vec{v}_f) = 0$,
 M o m e n t u m e q u a t i o n ,
 $\frac{\partial(\rho_f \vec{v}_f)}{\partial t} + \nabla \cdot (\rho_f \vec{v}_f \vec{v}_f) = -\nabla p + \nabla \cdot (\mu \nabla \vec{v}_f) + S$,
 E n e r g y e q u a t i o n ,
 $\frac{\partial(\rho_f C_{p,f} T_f)}{\partial t} + \nabla \cdot (\rho_f C_{p,f} T_f \vec{v}_f) = \nabla \cdot (k_f \nabla T_f) + q$.

Based on assumptions, these equations are modified for specific numerical simulation cases.

The conductive heat transfer within the battery cell is governed by the Fourier’s conduction equation,

$$\rho C_p \frac{\partial T}{\partial t} - \nabla \cdot (k \nabla T) = \dot{Q}$$

with convective boundary condition of, $k \frac{\partial T}{\partial n} = h(T_a - T)$,

where ρ denotes cell density, C_p denotes its specific heat capacity of the cell, T denotes the cell temperature, k denotes the cell’s thermal conductivity, $\partial/\partial n$ denotes the gradient in the direction of the outward normal to the boundary, h denotes the total heat transfer coefficient on the cell surface and T_a denotes the ambient (free-stream) temperature. For cylindrical batteries, the conduction equation is considered in cylindrical coordinates.

For the application the heat pipes, PCM and other cooling techniques of mist cooling, thermoelectric cooling etc., their respective standard governing equations are employed with the governing equations of the flow over the battery model given above.

4 Battery Heat Source Modeling

The thermal phenomena of a battery can be presented as an incremental set of models coupling with and without the electrochemistry of the battery as the electrochemical polarization also accounts for heat generation within the battery [38]. There are two groups of models based on the generation of heat whether being uniform or non-uniform.

4.1 Uniform Heat Source Models

According to the Helmholtz–Thevenin theorem, the series arrangement of voltage source V_0 and internal resistance R_s represents the battery as in Fig. 7. The rate of heat generation within a battery cell is given as $\dot{Q} = P = R_s I^2$ [W], where I is the current passing through the cell.

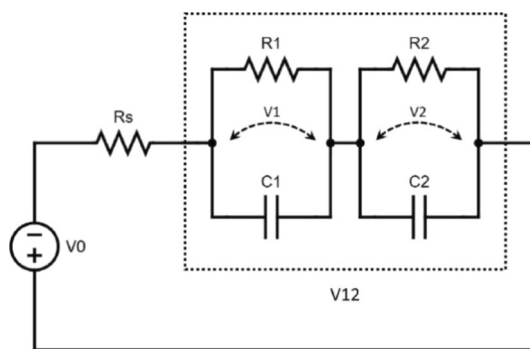


Fig. 7 Equivalent circuit of the battery: (voltage source V_0 and R_s alone) and full ECM (dashed circuit included) [39]

In the battery cell domain, where the generation of heat \dot{Q} being uniform throughout, the key challenge is the definition of the value for R_s as it affects the efficiency, power output and heat generation during charging and discharging cycles, and the other parameters can be approximated by their mean values. The two methods of the estimation of internal resistance R_s are given as follows [39]:

4.1.1 Manufacturer Specified R_s (Constant- R_s)

The preliminary (or) initial estimates of heat generation rate can be facilitated by the battery manufacturer provided internal resistance R_s as it does not require any measurements. The dynamic factors of temperature, state of charge and the current drawn cannot be accounted in this preliminary estimation along with the aging effects of the battery.

4.1.2 State of Charge Dependent R_s (SoC – R_s)

As mentioned above, the internal resistance R_s along with V_0 the open circuit voltage are dynamic with the temperature and State of Charge (SoC) of the battery in reality. The current pulses measured at the points of sudden voltage drops from a Discharge Pulse Power Characterization (DPPC) test or any equivalent tests gives the SoC-dependent values of R_s values for the estimation of heat generation rate [40].

4.2 Generalized Heat Source Model

The two general heat generating sources of the battery are the internal resistance of the cell related with the electrochemical reactions named as ohmic heating (Q_{ohmic}) or over potential heating and other is entropic heating ($Q_{entropy}$) which is due to the change in entropy during the conditions of charging/discharging cycles. Therefore, the generalized heat source model is given as, $\dot{Q} = Q_{ohmic} + Q_{entropy}$

$$Q_{ohmic} = I(V_0 - V) = I^2 R_e \text{ and } Q_{entropy} = -I \left(T \frac{dV_0}{dT} \right).$$

$$\text{Therefore, } \dot{Q} = I^2 R_s - I \left(T \frac{dV_0}{dT} \right),$$

where V is the cell voltage, V_0 is the open circuit voltage and the gradient $\frac{dV_0}{dT}$ is the entropic heat coefficient which is a function of state of charge (SoC).

Bernardi et al. [41] developed this general simplified ‘thermal–electrochemical’ model based lumped parameter approach. Because of the simple and speedy estimation of heat generation with reasonable accuracy, it is more convenient for initial approximations and system-level modeling of battery. But it neglects the effects of,

- Phase change within the electrodes in the cells due to expansion and contraction of the electrode materials during charging and discharging conditions which may affect the performance of the battery.
- Mixing of the fluids in the cell causing temperature heterogeneity and non-uniform concentrations whereas here an assumption lumped parameter of temperature and concentration is considered.
- Gradient and Localized effect of temperature and concentration due to the variation of heat dissipation and ion transport in the battery cells.

4.3 Nonuniform Heat Source Models

The heterogeneous nature of battery with non-uniform heat generation in real applications lead to the development of a novel approach of Multi-Scale Multi-Domain, MSMD [42] in modeling the battery cell considering various physics of thermal, electrical, and electrochemical in various solution domains of electrodes, electrolyte, and separator. The physics can be coupled to study the effects of the influence of one domain on the other. The process occurring from microscale level to the macroscale level in the battery cell can be accounted in the MSMD approach to represent the behavior of the cell [43]. Therefore, the heat source model for MSMD approach is,

$$\frac{\partial(\rho_f C_{p,f} T_f)}{\partial t} - \nabla \cdot (k \nabla T) = \sigma_+ |\nabla \phi_+|^2 + \sigma_- |\nabla \phi_-|^2 + \dot{q}_{Ech} + \dot{q}_{short} + \dot{q}_{abuse},$$

where σ_+ and σ_- are the effective conductivities for the positive and negative electrodes, ϕ_+ and ϕ_- are phase potentials for the positive and negative electrodes, \dot{q}_{Ech} is the electrochemical reaction heat due to electrochemical reactions at the electrode–electrolyte interfaces, \dot{q}_{short} is the rate of heat generated during internal short-circuit of the battery and \dot{q}_{abuse} is the rate of heat generated during thermal runaway reactions leading to catastrophic failure.

In addition, MSMD is coupled with the Newman–Tiedemann–Gu–Kim model (NTGK) [44] which describes the battery’s electrochemical process as a function of Degree of Discharge (DoD) which reflects the State of Charge (SoC) of the battery by taking the polarization behavior of the battery into consideration. The algebraic NTGK model provides an insight on the steady-state description of the electrochemical behavior of the battery considering that the any alterations in the current discharged from the battery is instantly reflected on the voltage of the battery. But, in real application the algebraic model may not be accurate in capturing the non-uniform heat generation as the variation of voltage with altering current is dynamic not a steady state

phenomenon. This paves the way towards the Equivalent Circuit Model, ECM [45] approach representing the battery as a network of resistors, capacitors, and voltage sources predicting the dynamic behavior of voltage with current during the cycles of charging and discharging in the battery, providing an accurate modeling of the heat source model of the battery [46].

5 Numerical Analysis

5.1 Air Cooling System

The crucial parameters of peak temperature and thermal homogeneity is numerically investigated employing ANSYS FLUENT software solving the Reynolds-averaged Navier–Stokes (RANS) equations and $k-\epsilon$ turbulence transport equations for newly designed battery modules with the cell holders' jacket fins by Obula Reddy [47]. The temperature gradient resulted 0.26 °C for the base design without the modifications whereas 0.04 °C gradient in new design developed ensures the homogeneity of temperature in the new design module. In addition, the peak temperature in the new design is observed to be 1 to 4 °C lower than base design.

Osman et al. [48] optimized the intracellular distance (20, 25, 30, 35, and 40 mm) using FLOEFD of a 18,650 Lithium-ion (NCA) battery to 20 mm and 25 mm, as a decline in the energy density is evident with increase in distances. For 20 mm intracellular distance module have a maximum temperature of 41.89 °C and adding a honeycomb shaped metal insert (Al, Cu, and SS-312) with a 0.5 mm thick enclosure of plastic in a 14-cell battery module as in Fig. 8 influenced the thermal performance by limiting the peak temperature to 37.39 °C and maintaining

a temperature homogeneity of 0.59 °C to support equal aging at 1C charging rate at 25 °C.

Alharbi et al. [49] arranged the batteries in rectangular, lozenge, and triangular form in the pack and highlights the importance of arrangement of the batteries on enhancing the performance of air-cooling strategy. In spite of depicting higher resistance to air flow by showing an increased pressure drop, the triangular arrangement obtained an excellent thermal control by lowering peak and mean temperature as in Fig. 9.

The numerical investigation on the cylindrical Li-ion batteries by Mesut et al. [50] using ANSYS CFX implies that the airflow in axial direction is more efficient than the cross-flow for temperature distribution and cooling air at 30 °C is insufficient when the module is in aligned and staggered configurations, and wider configuration affects thermal performance negatively when the aluminum fins on the surface of longitudinal side is re-designed in rectangular form and highlights that the fins can enhance only the dissipation of the heat avoiding accumulation in the battery but don't maintain a homogenous temperature distribution.

Numerical investigation using the standard model of $k-\epsilon$ turbulence with the SIMPLEC solver on the cylindrical actively air-cooled Li-ion battery pack by Saechan et al. [51] optimized the performance of the strategy during the discharge process. A cooling gap of about 1.5 mm is concluded optimum to enhance the performance of cooling and further enhances with the increased inlet velocity. For the case of simple structured battery pack with fast-discharging rate of 2C-rate, it is concluded that the thermal management utilizing the forced-air cooling strategy is seemingly not sufficient.

Different air-cooling techniques by changing the inlet and outlet position as shown in Fig. 10 studied by Jiaqiang et al. [52] of a 60-cell Li-ion battery pack discharging at 1C rate

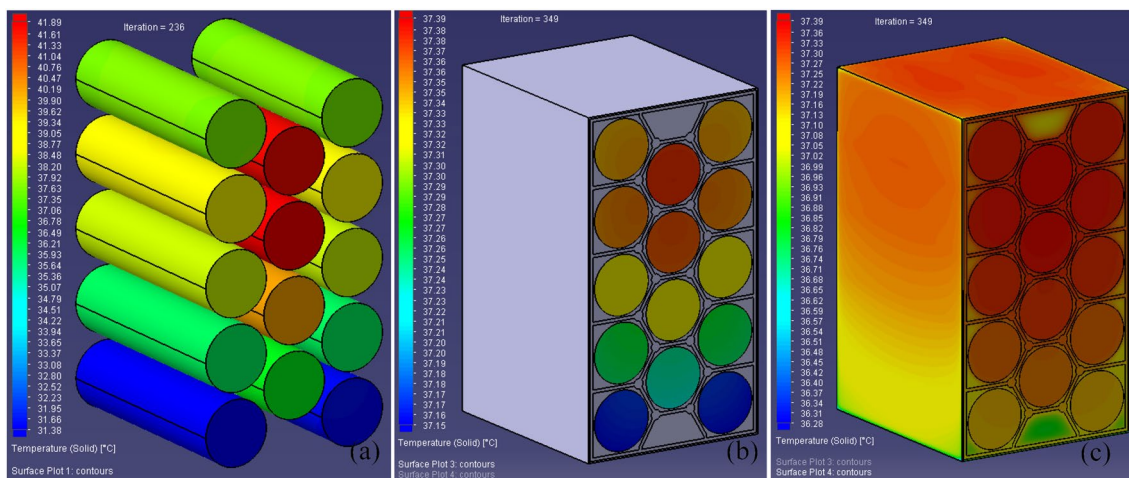


Fig. 8 Temperature contours: a open module, b module inside enclosure supported with an aluminum honeycomb insert, and c enclosure [48]

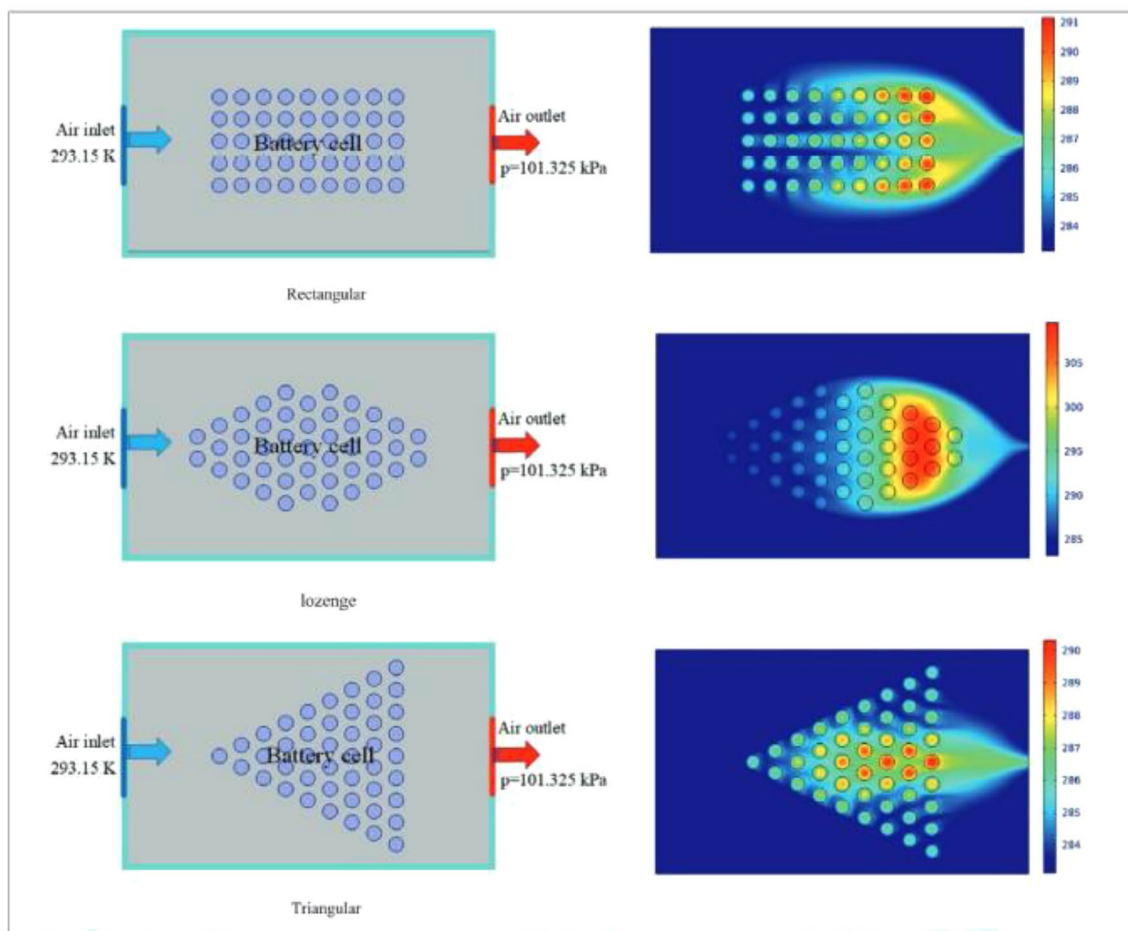
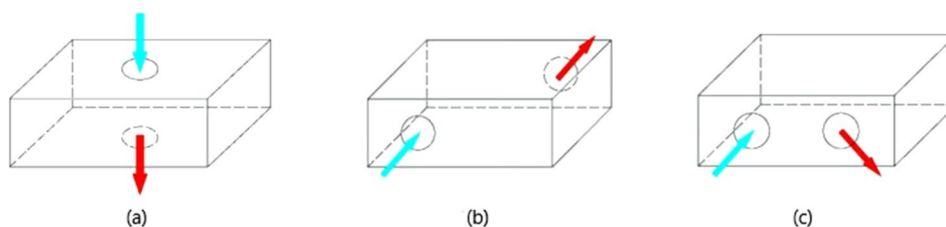


Fig. 9 Schematic and temperature contours of different arrangements of battery [49]

Fig. 10 Different positions of inlet and outlet: **a** top inlet and bottom outlet, **b** inlet and outlet on different lateral sides, and **c** inlet and outlet on same lateral side [52]



with 25 °C initial temperature observes ineffective thermal performance with the model designed with top inlet and bottom outlet whereas lateral models were better. Different side inlets and outlets had 3.2% and 8.9% lower T_{\max} and ΔT respectively compared with the same side for exit and incoming of air. Addition of baffles further lowered T_{\max} and ΔT by 5.7% and 28.8% respectively as shown in Fig. 11.

Saw et al. [53] ensured an effective management of the thermal behavior on analyzing 38,129 cell air-cooled Li-ion battery pack by maintaining the average deviation of about 2.6 °C, and 39.2 °C peak core temperature when several

components, such as plenum at the intake and exhaust points of air, bus bars between the cells made of copper and holding plates integrated with holes for ventilation, for enhancing the thermal performance is included. In spite of high thermal performance, even at higher cooling air flow rate of 40 g/s some hotspots are pointed on the battery pack especially on the center and front end due to insufficient distribution of cooling air in the battery pack, highlights the need of proper flow channels to distribute the incoming cool air.

Yu et al. [54] numerically described the dual air-cooling strategy combining the conventional ducts having channels

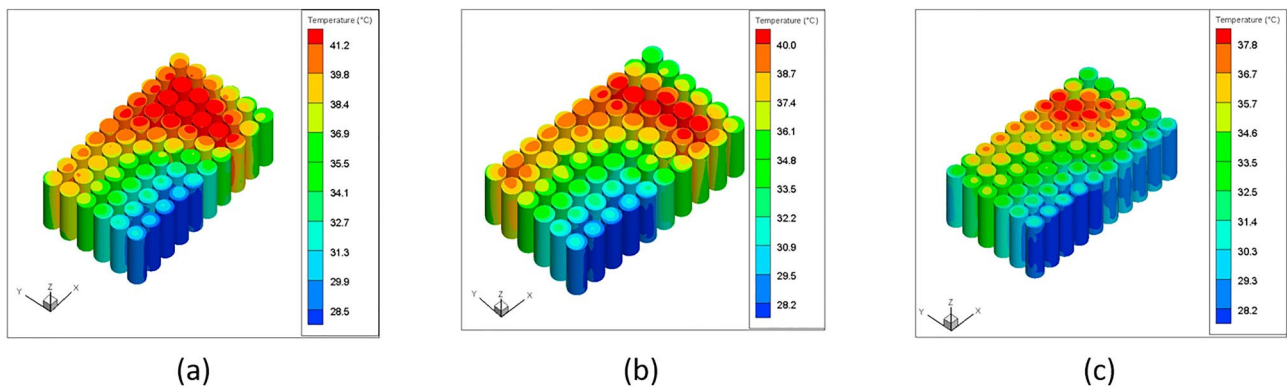


Fig. 11 Temperature contours for inlet and outlet on **a** same lateral sides, **b** different lateral sides and **c** different lateral sides with baffle [52]

for cooling of the battery with the jet cooling strategy to reduce the accumulation of heat in the middle portion of the battery with inlet channels and fans which are independent from the traditional strategy. The application of this dual approach to the original traditional pack declined 9 °C in the peak temperature and ensures homogeneous temperature distribution as shown in Fig. 12.

Wang et al. [55] numerically investigated the effects of the positions of the fan in the performance of the forced air-cooling strategy concluding enhanced performance with fan at the top of the battery pack. On the analyzing different structures of arrangement of batteries in the pack, the hexagonal arrangement of batteries is superior with the characteristics of effective space utilization and thermal performance

but when considering the characteristics of cooling capability and cost, the cubic arrangement is better.

Fan et al. [56] numerically investigated the influence of different arrangements of the prismatic pouch lithium-ion cells on the performance of the air-cooling strategy resulting a configuration of 3 mm even spacing between each cell and 40.8 m³/h air flow rate achieved a balance between the factors of parasitic power consumption by the fan with the thermal performance factors as when the cells are arranged as in Fig. 13a cooling are experienced on both sides of the cell leading to the rise in maximum temperature enhancing the uniformity with the increase in the gap between the cells at a constant airflow rate and increase in airflow rate reduced both the peak temperature and the uniformity as in Fig. 14. Though enhancing the thermal homogeneity, the

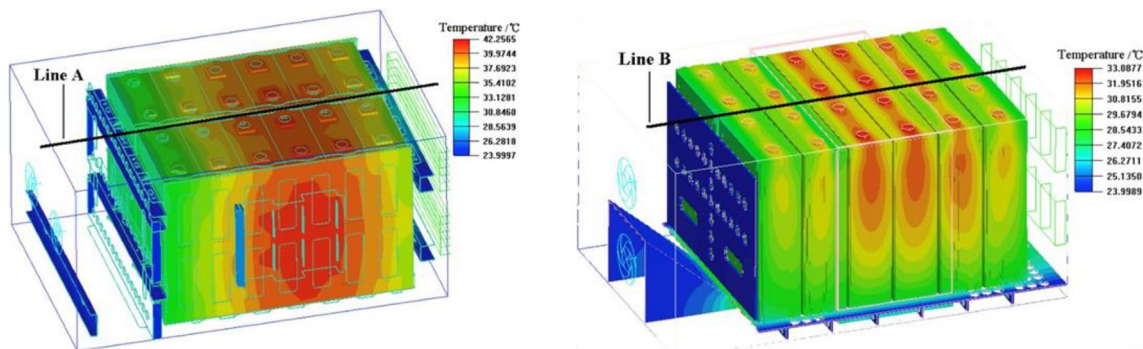


Fig. 12 Temperature contours of the original (A) and two-directional (B) air flow cooling pack at the end of 1C rate discharge [54]

Fig. 13 Schematic of the **a** two-side cooling and **b** each cell cooled only from one side [56]

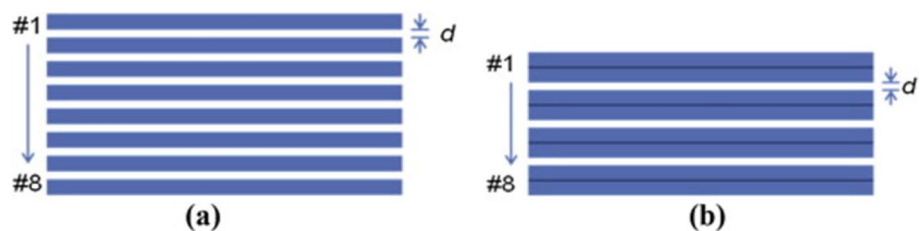


Fig. 14 Temperature contours for even spacing of 3 mm at different air flow rates [56]

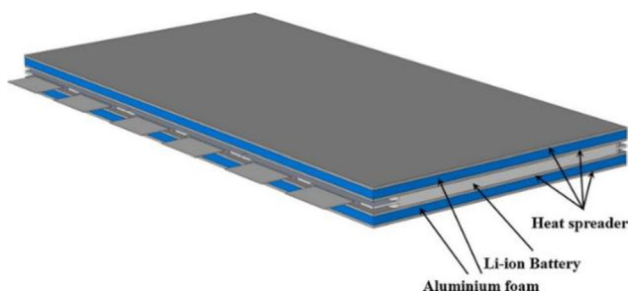
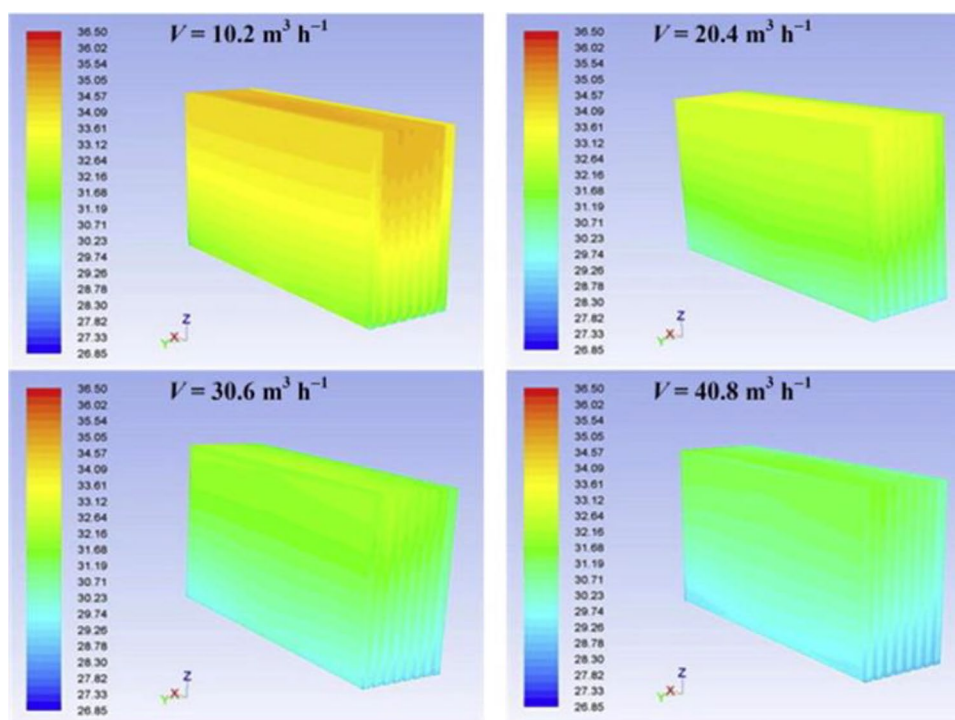


Fig. 15 Design of cold plate with aluminum foam fitted for pouch type battery [57]

strategies of employing one-side cooling and uneven cell spacing failed in the reduction of peak temperature.

The numerical investigation on the air-cooling technique of a pouch type Li-ion battery exhibited an enhancement in the thermal performance with the application of foam made of aluminum, whose porosity impacts the temperature and pressure drop of the system, forming a cooling plate with the aid of heat spreaders on both the sides as in Fig. 15. Saw et al. [57] concluded that the reduced porosity exhibits a declined temperature on the battery surface and the pressure drop across the flow of air, but it negatively affects the homogeneous distribution of temperature on the battery. Therefore, on performing various numerical simulations, at cooling air flow rate of 20 g/s a balance between the thermal performance and pressure

drop struck when employing a 10 PPI aluminum foam having a porosity of 91.9%.

Shahabeddin et al. [58] integrated the foam of aluminum in the air flow channels enhancing the performance of the air-cooling strategy in the Li-ion battery by examining four different cases as in Fig. 16 where the airflow channel length filled with 70% of porous metal foam with a permeability of 10^{-7} and porosity of 0.85 from the channel outlet (case 3) is optimal to obtain better thermal performance.

5.2 Liquid Cooling System

5.2.1 Cold Plates

Sarvar et al. [59] on studying the thermo-hydraulic performance of the cold plates on embedding a porous substrate in the mini channels for a 3C discharge rate battery pack. Non-porous and half-porous substrate in the channels delivered a better cooling performance when the coolant flows in counter current direction. The effect of full porous structure in the mini channels is completely exhibited when there was parallel flow of coolants such that declining the maximum temperature to 38.12 °C with better temperature distribution and accounting for a 17.5% increased performance at a coolant velocity of 0.05 m/s than counter flow as in Fig. 17.

The cooling performances of 65 Ah pouch-type batteries arranged in a series of four are numerically studied by Adeniran et al. [60] with ambient cooling, cooling plate on single side and double sides of the battery pack using water

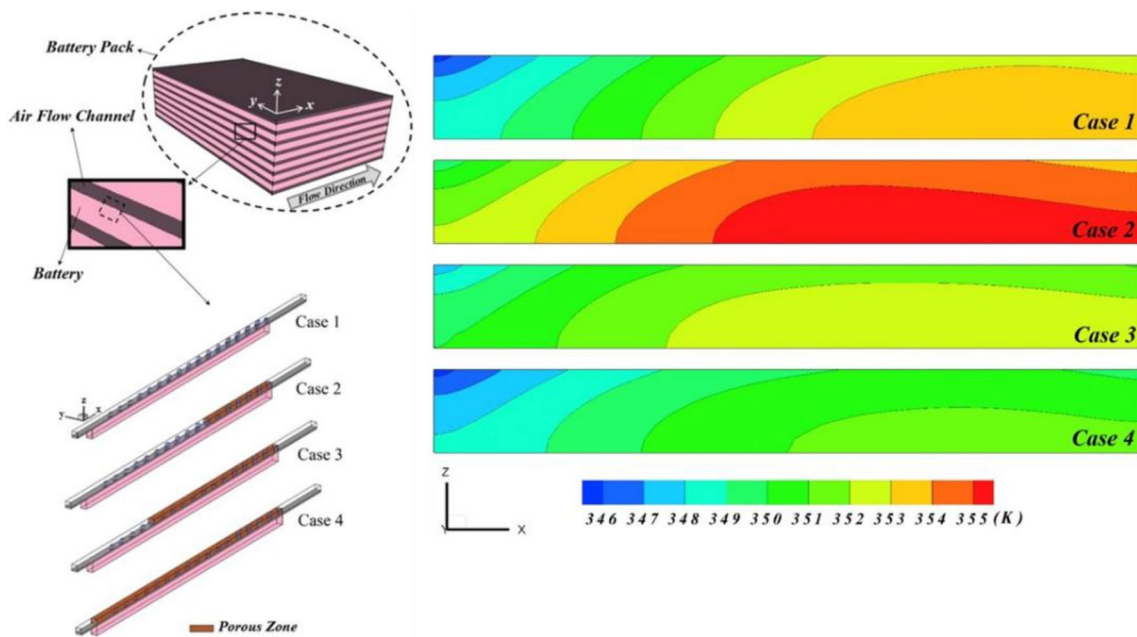


Fig. 16 Schematic and temperature contours of the different cases of air-cooling channels with metal foam [58]

Fig. 17 Temperature contour of the cold plate for different porous structures at 0.05 m/s coolant velocity with **a** parallel flow and **b** counter flow [59]

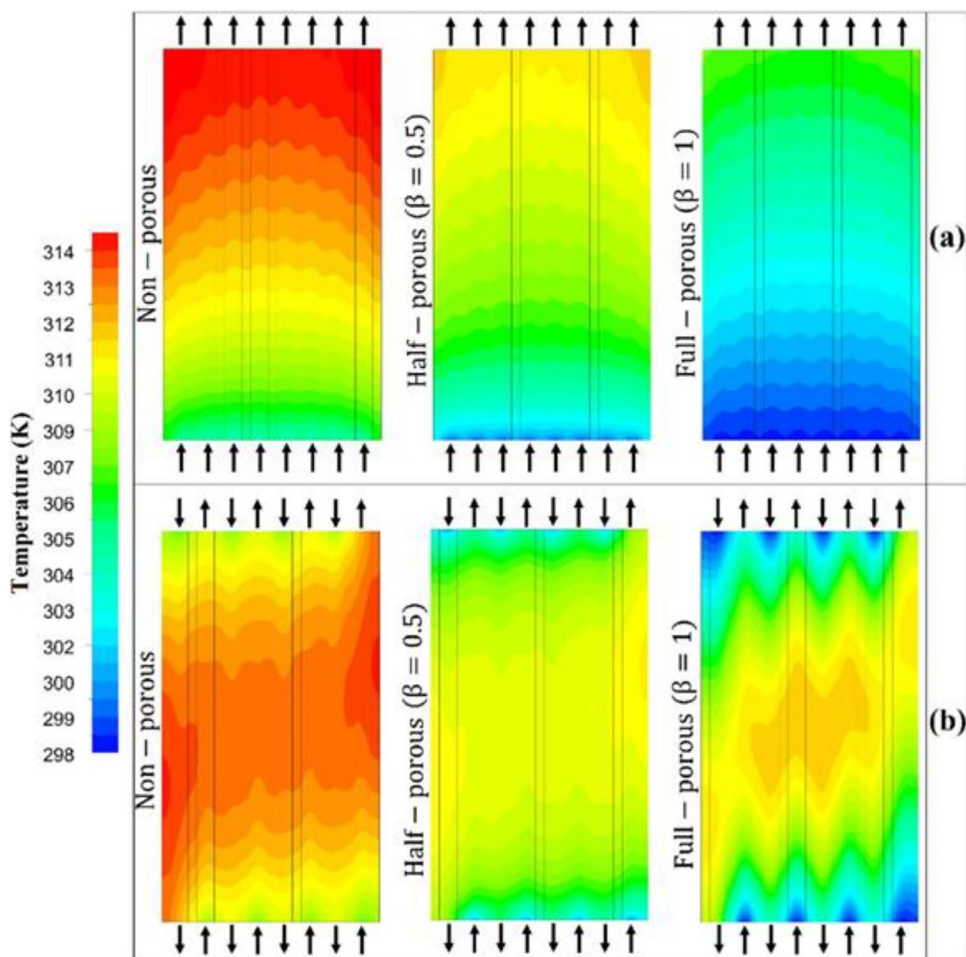


Fig. 18 Temperature distribution **a** with double side, and **b** with single side cooling plate [60]

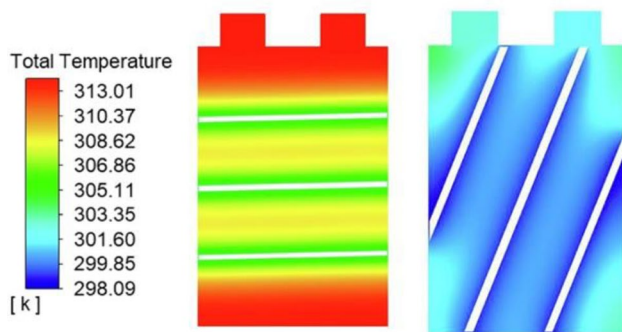
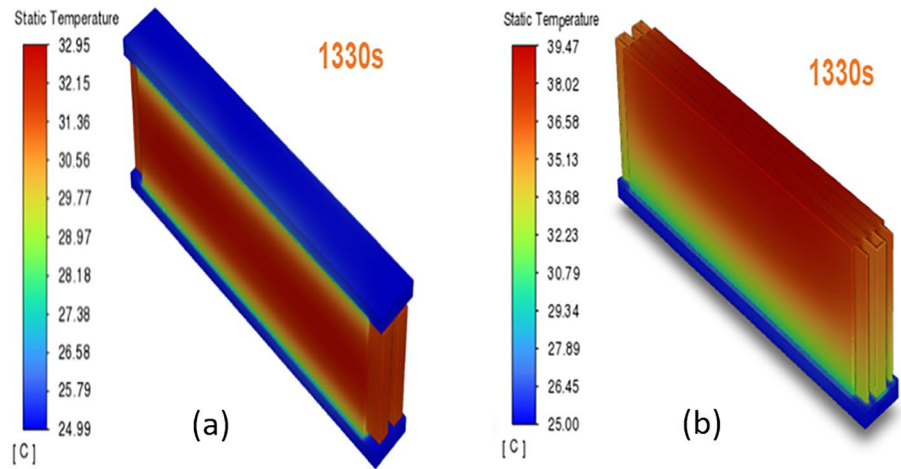


Fig. 19 Temperature distribution contours for 1.4° and 68.9° inclined channels [61]

flowing at 0.33 kg/s as coolant for fast charging cycles of 1.98 C-rate at an ambient of 50 °C using ANSYS FLUENT. A cooling plate of 10.5 mm height declines 10 °C temperature when installed on single side of the battery pack as in Fig. 1b. The heterogeneous distribution of up to 10 °C temperature on utilizing cooling plate on single side lead to the installation on double sides showing 50% decline of temperature deviation to 5 °C with counter current direction of coolant flow along with the 7 °C reduction in peak temperature as in Fig. 18. The double side configuration is widely adaptable for various flow and discharge conditions.

Investigation of the mini-channels having various geometries by Verma et al. [61] shows a homogeneous distribution of temperature with diagonal and vertical mini-channels compared to horizontal mini-channels as shown in Fig. 19 and geometrical parameters of aspect ratio and inclination angle of the channels are optimized to 1.7 and 4.9° respectively employing Technique for Order Preference by Similarity to an Ideal Solution (TOPSIS Analysis) for 40 °C ambient conditions and 0.85 W parasitic power requirement

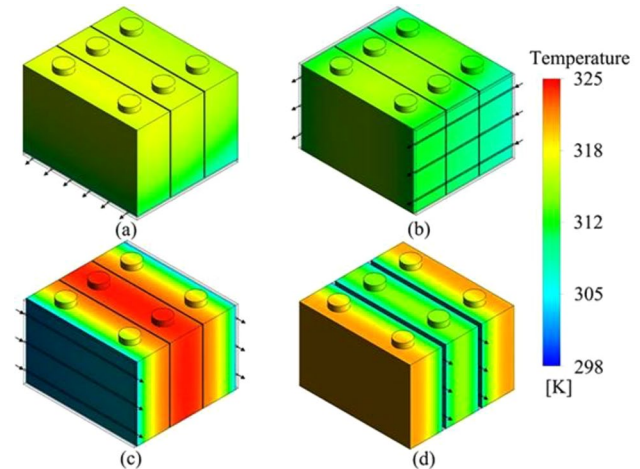
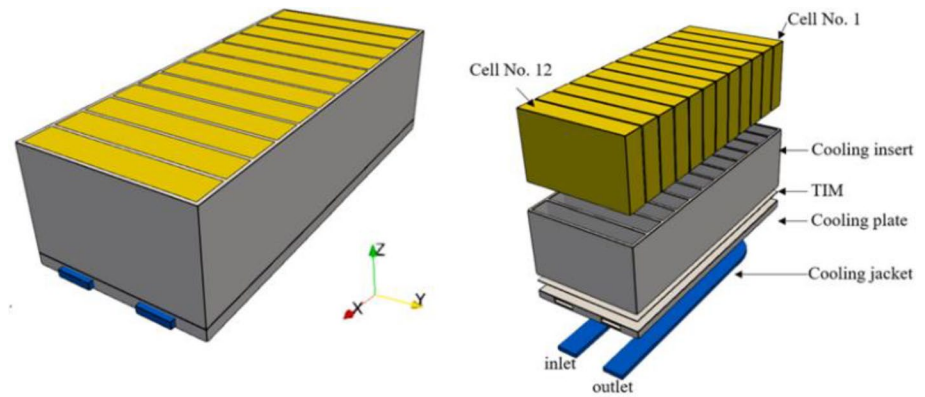


Fig. 20 Thermal response on placing cooling plates on the **a** Bottom face, **b** Side face, **c** Main face, and **d** Main face medium [62]

for coolant velocity of 0.13 m/s in maintaining the peak temperature at 313 K.

The cold plates with 4 Tesla valve shaped elements on each of four mini channels are numerically investigated by Lai et al. [62] for the forward and backward orientation of Tesla valve and various positions of the cold plate in the battery pack with 2C-discharge rate. A 5.6 °C decline of maximum temperature in the cooling plate position is changed from main face (c) to side face (b) as in Fig. 20 improving temperature homogeneity by declining ΔT by 8.5 °C. The orientation of the valves had impact on the pressure drop thereby on the parasitic power consumption where the forward oriented is advantageous. The forward oriented valve is superior to the straight channels in maintaining a 38 °C peak temperature with a deviation of 7 °C with coolant flowing in counter current directions.

Fig. 21 Schematic of the battery module and its components [63]



A 3 mm cooling insert integrated prismatic NCM (Nickel Cobalt Manganese) Li-ion battery module as in Fig. 21 investigated at steady-state conditions using conjugate heat transfer solver of Open Foam software showed an 15.6% enhanced heat transfer into the thermal interface material in comparison with the module having no insert. In addition, Han et al. [63] depicted a reduced temperature difference of up to 4 °C at higher discharge rates, thereby enhancing the battery's performance.

The influence of cold plate with different shaped serpentine channels as in Fig. 22 on the cooling performance studied by Guo et al. [64] using STAR CCM+ at initial conditions of 298 K temperature and 5 W/m²/K convective heat transfer coefficient shows that the parallel-spiral channel cooling plate as shown in Fig. 23 offers better comprehensive performance of temperature, and pressure drop under steady-state simulation at 0.04 kg/s mass flow rate and constant heat generation effect of 1C rate using *k-ε* turbulence model.

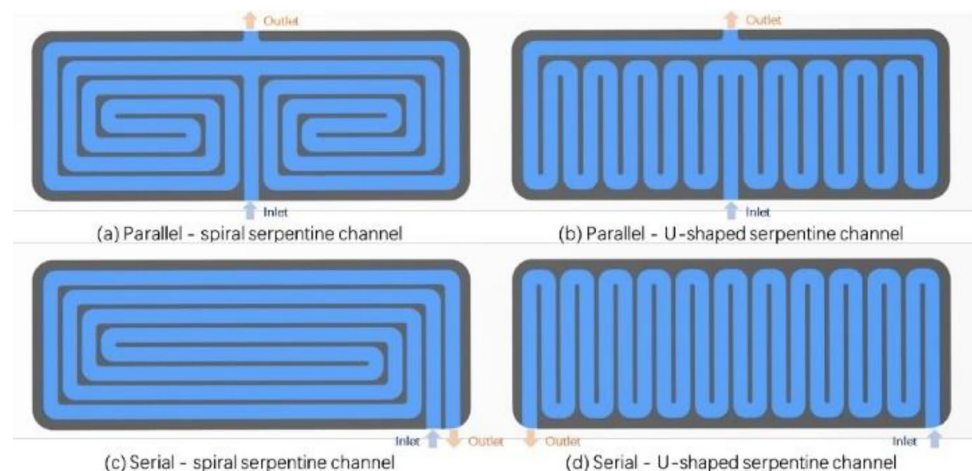
The numerical investigation on various shapes of cold plate channels of single-S (SSCP) and double -S (DSCP) by Wei et al. [65] on the thermal performance and pressure drop as in Fig. 24 shows that on varying the mass flow rates of the

coolant, ambient and rate of discharge DSCP provides better temperature distribution than SSCP as in Fig. 25 though both plates depict a similar peak temperature of the battery. The implementation of DSCP reduced the pressure drop by 73.88% compared with SSCP. The overall thermal performance evaluation criterion (PEC) which defines the heat transfer and flow resistance, was better for DSCP at all conditions and very high at a 3C discharge rate, 1 g/s water-glycol coolant flow rate, and 20 °C ambient conditions.

Tang et al. [66] focused on the development and analysis of reduced weight cooling plates for the prismatic batteries. Slender tubes of different encircling modes as in Fig. 26 designed as light-weight cooling strategy reduces the T_{max} and ΔT to 38.28 and 4.23 °C for the encircling mode of D22 having increased tube length at a coolant velocity of 0.25 m/s and 2.5 mm inner tube diameter. The T_{max} and ΔT is further reduced to 34.97 and 4.04 °C respectively with full encirclement mode D24 at 0.5 m/s and 2 mm. The encircling mode of D22 and D24 shows weight ratio of the cooling system to the battery module as 1.88% and 2.00% respectively, exhibiting the development of lightweight system.

Deng et al. [67] states that the change in the flow direction of the coolants improves the homogeneous distribution of

Fig. 22 Different shapes of serpentine channel cooling plates [64]



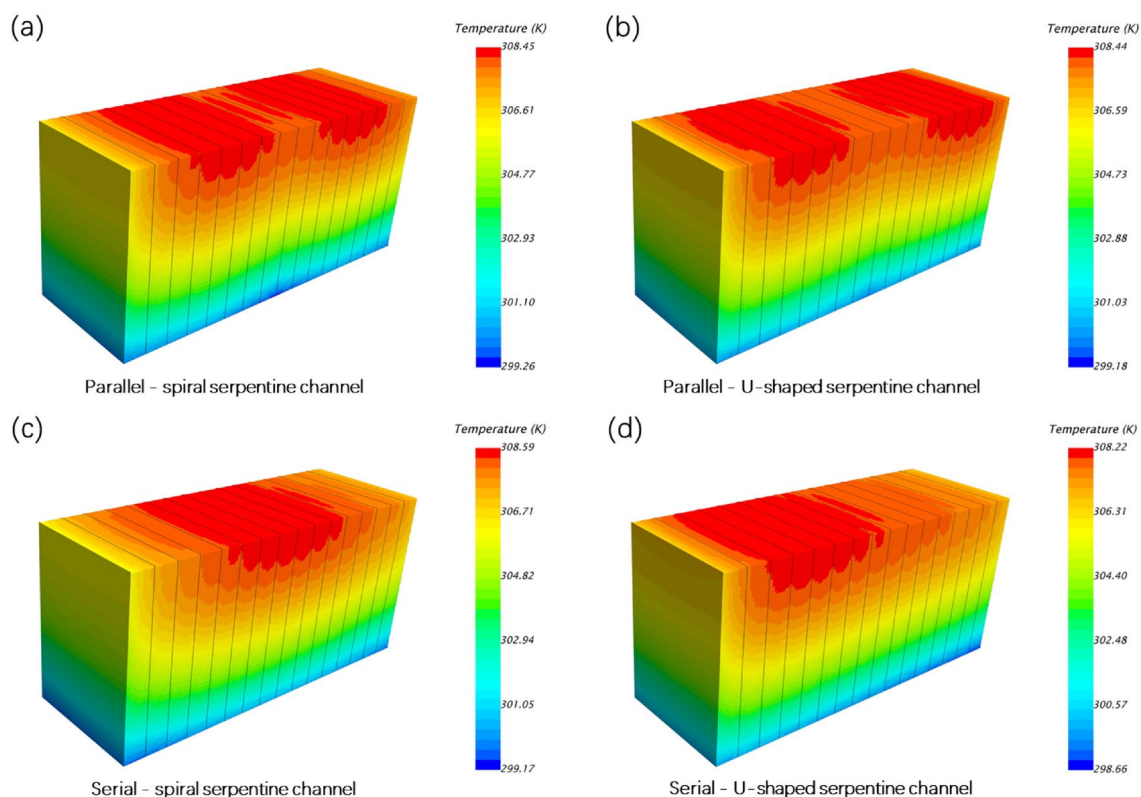


Fig. 23 Thermal contours of the module for different channel arrangements [64]

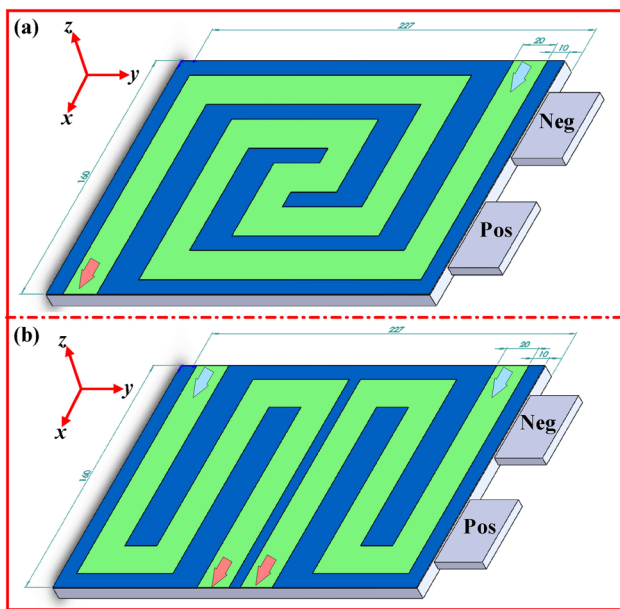


Fig. 24 Shapes of mini channel in the cold plate: a single S and b double S [65]

temperature from Design 1 to Design 6 as shown in Fig. 27. For increased coolant flow of 1 g/s, a maximum temperature of 27.67 °C and 32.17 °C is depicted by a four prismatic battery pack after rate of discharge of 3C and 5C respectively. The thermal performance can be comparatively improved by the close arrangement of cooling plates, the channels aligned to the center of battery results a peak temperature of 27.59 °C and 31.96 °C at the end of 3C and 5C discharge respectively as in Design 532.

During the examination of channel heat sinks resembling trees at 4C rate of discharge, Liu et al. [68] achieved 34.21 °C peak temperature with 5.35 °C temperature deviation and 11.26 Pa pressure drop. These results demonstrated superior performance compared to straight structures. By optimizing the inlet width and slant angle of the channels they further reduced the temperature to 33.69 °C, temperature difference, to 4.86 °C and pressure drop to 17.99 Pa with optimization results that deviated by less than 1% from CFD results.

To minimize temperature non uniformity within battery modules Zhao et al. [69] conducted numerical studies on two approaches for channeled liquid cooling. The first approach involved shortening flow paths using many channels while the second approach focused on increasing contact areas between batteries and serpentine channels

Fig. 25 Temperature contour of the battery with SSCP and DSCP under different coolant mass flow rates [65]

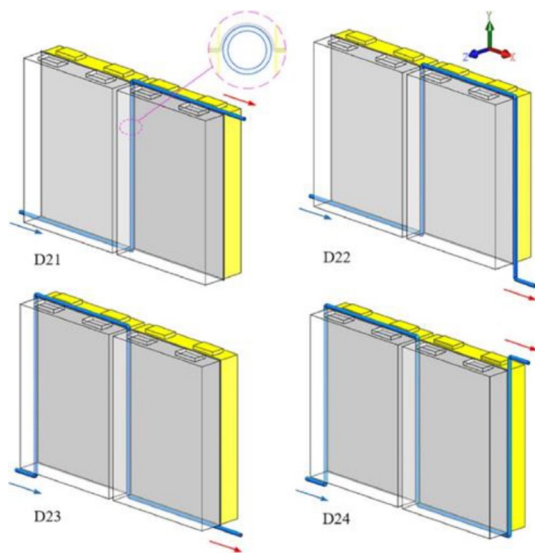
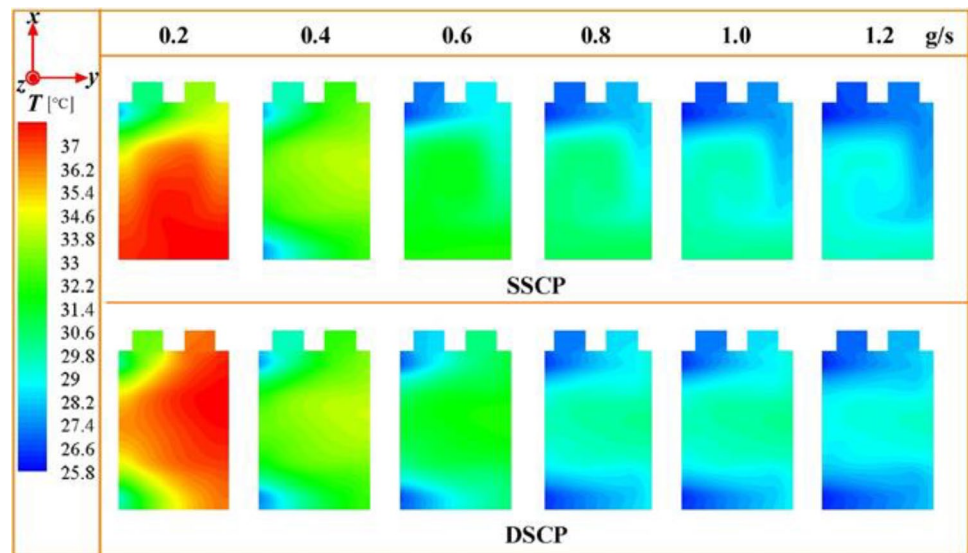


Fig. 26 Different encircling modes in battery module for D21–D24 [66]

along the streamwise direction of flow path. These strategies resulted in temperature differences of 2.2 K and 0.7 K during a discharge rate of 5C and stresses that these findings should not be considered as the ways to minimize temperature, non-uniformity in battery modules as there are other approaches available.

At extreme operating conditions of 40 °C and 1C discharge rates, Xu et al. [70] numerically investigated novel cooling plates with channels resembling T-shape. A uniform distribution of water in this bifurcation structure with 0.94 index as shown in Fig. 28 for prismatic LiFePO₄ battery modules showing a drop in temperature from 90 to 35.6 °C and deviation of temperature from 20 °C to about 1.5 °C as

shown in Fig. 29 with inlet conditions of 30 °C, 1 g/s. It is highlighted that the thermal performance had less impact with the varying water flow rates whereas the change in inlet temperature to 28 °C declines the peak temperature to 33.5 °C.

Furthermore, a helical duct designed for Li-ion batteries with 5C rate of discharge was numerically examined by Zhou et al. [71]. Increasing the coolant mass flow rate from 1×10^{-5} to 3×10^{-4} kg/s at a depth of discharge (DoD) of 100% effectively reduced the temperature from 66.7 to 30.8 °C resulting in decreased temperature difference of 5.4 °C as in Fig. 30. The impact of cooling performance, on the pitch and quantity of ducts was found to be negligible. However, when the direction of coolant flow was modified as in Fig. 31, case 4 showed an improvement of maintaining by 30.5 °C peak temperature and 4.6 °C temperature difference at the end of discharge.

When combining a silica cooling plate with copper mesh for an air-cooling system as in Fig. 32, results an effective cooling solution. Improved cooling enhances the efficiency of lithium-ion batteries when they undergo a 5C discharge. Optimal performance is achieved with a silica cooling plate that has a thickness of 1.5 mm and an air velocity of 3.5 m/s. Based on simulations Li et al. [72] suggested that placing the fan at the side of the battery yields excellent results compared to placing it at the back side allowing for more effective forced cooling as an average temperature of 49.76 °C and 50.19 °C was observed with five batteries under 1.5 mm cooling plate thickness, 5 m/s velocity with two fans and one fan respectively.

The numerical analysis of cold plate water cooling systems having mini channels was conducted by Panchal et al. [73] in ANSYS FLUENT employing $k-\epsilon$ model. The investigation considered discharge rates of 1C and 2C, 5 °C, 15 °C

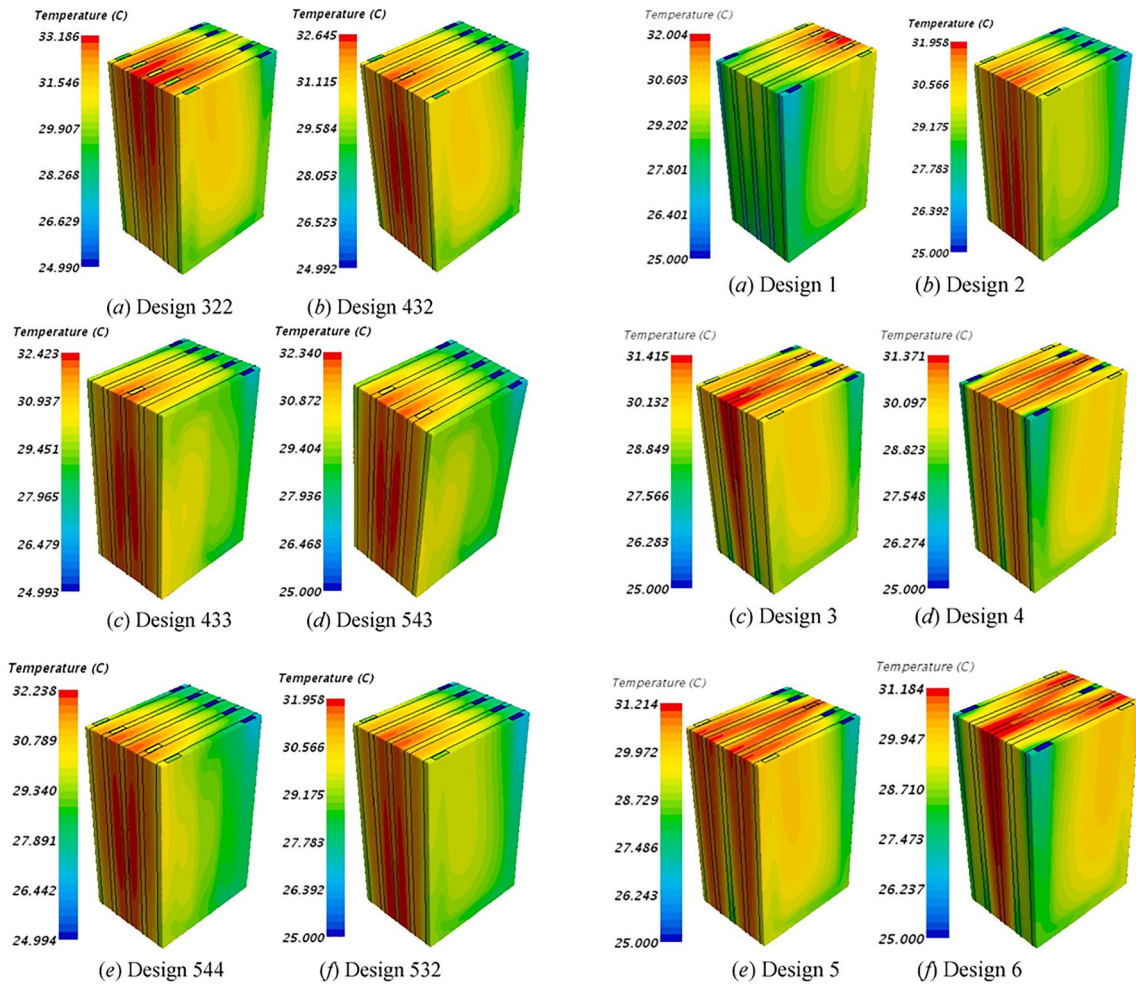


Fig. 27 Temperature contours with different channel number distributions and different cooling directions [67]

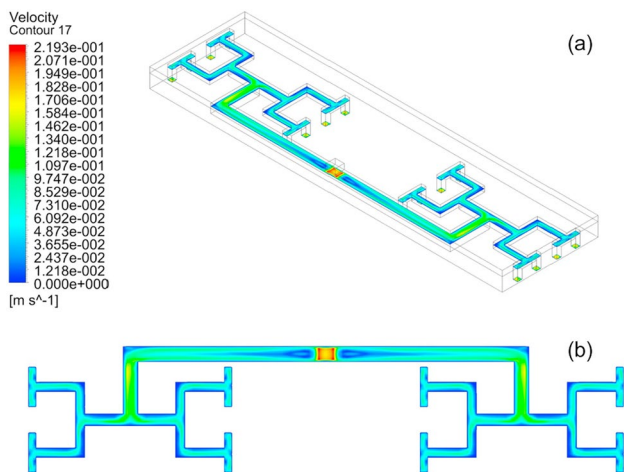


Fig. 28 Velocity contour of water distribution a oblique, and b top view [70]

and 25 °C ambient temperatures. The results clearly indicate that as the C rates and operating temperatures increase both the temperature distributions and maximum temperature within the channel cold plates also rise.

In order to determine the heat generated by the internal resistance functions of battery in conjunction with the entropic heat coefficient STAR CCM+ software is employed. This information was then utilized in simulating the thermal behaviour under cooling conditions of a battery pack over time by De Vita et al. [74]. The findings of thermal behaviour demonstrate thermal limits of implementing liquid cooling plates (Fig. 33).

Based on the research of Zhen et al. [75], it is determined that a cold plate with five channels is optimal for a Li-ion battery pack as increasing the number of channels over it does not provide advantages. Furthermore, utilizing a 2-channel plate ensures that the peak temperature remains below 40 °C even after, half of the discharge time. Additionally, increasing 3 to 6 mm channel width and flow rate results in a reduction in pressure drop by 55% (Fig. 34).

Fig. 29 Temperature contour **a** at the end of discharge, and **b** with designed cooling plate [70]

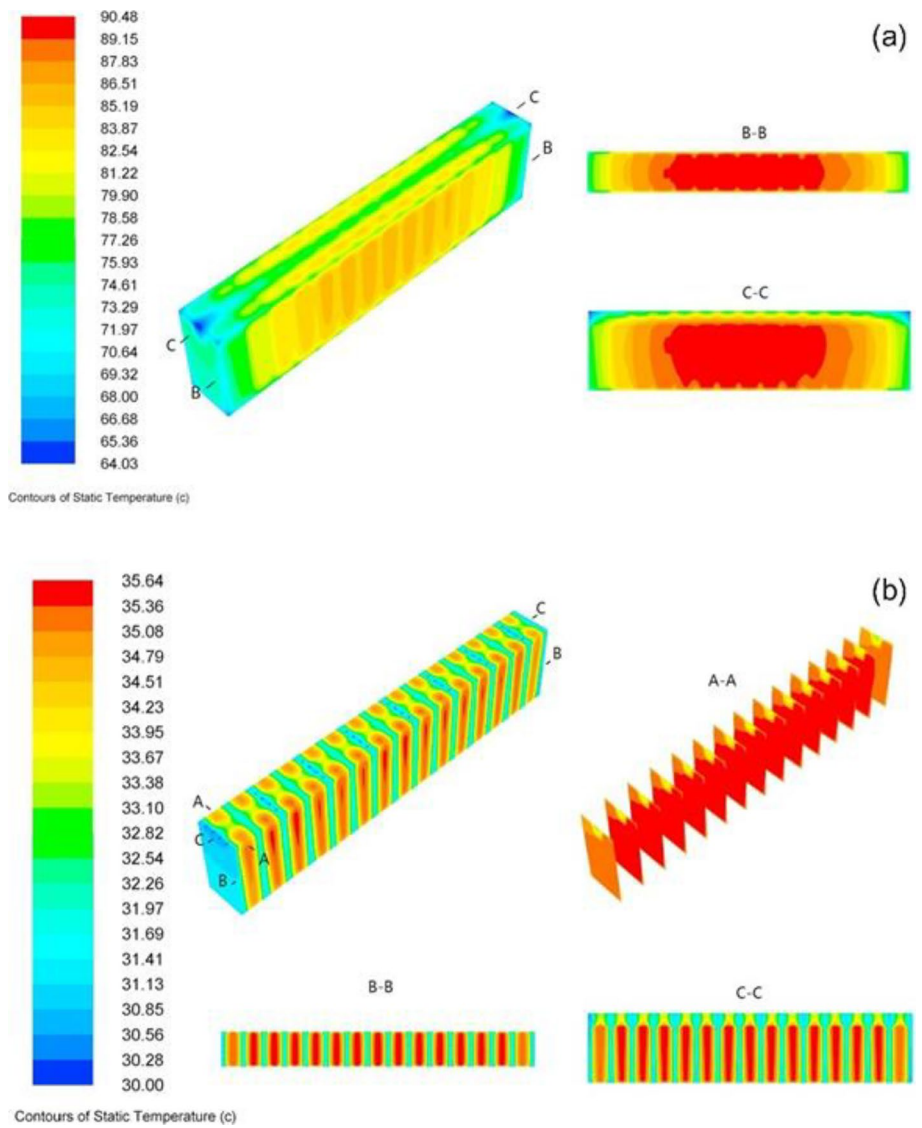
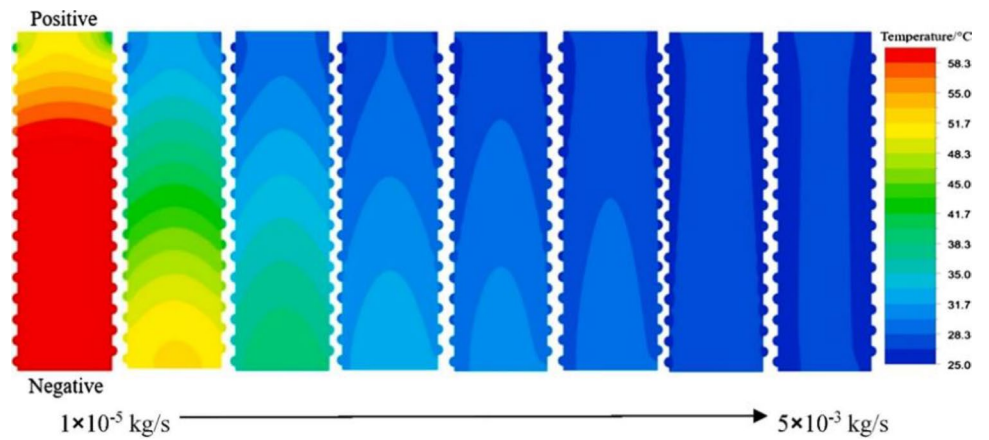


Fig. 30 Temperature contour of battery for increasing mass flow rates of coolant [71]



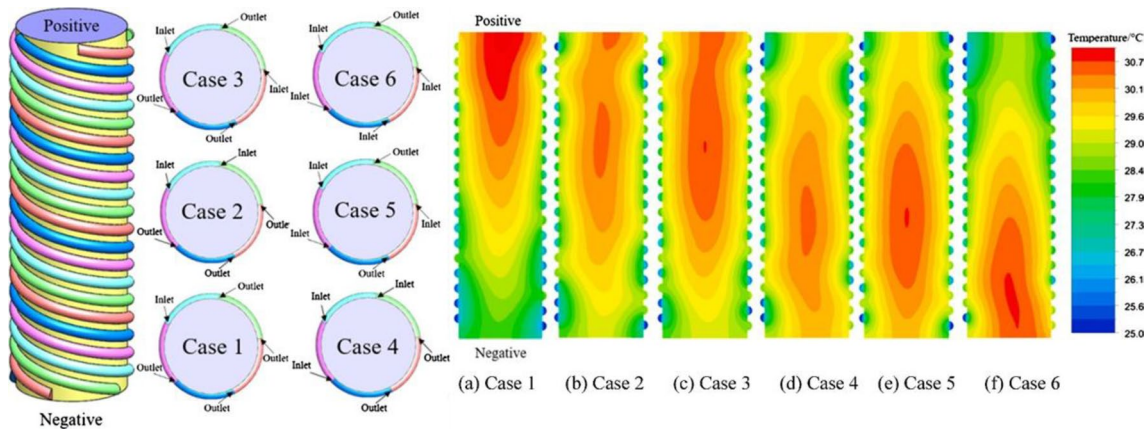


Fig. 31 Schematic and Temperature contour of different flow direction cases [71]

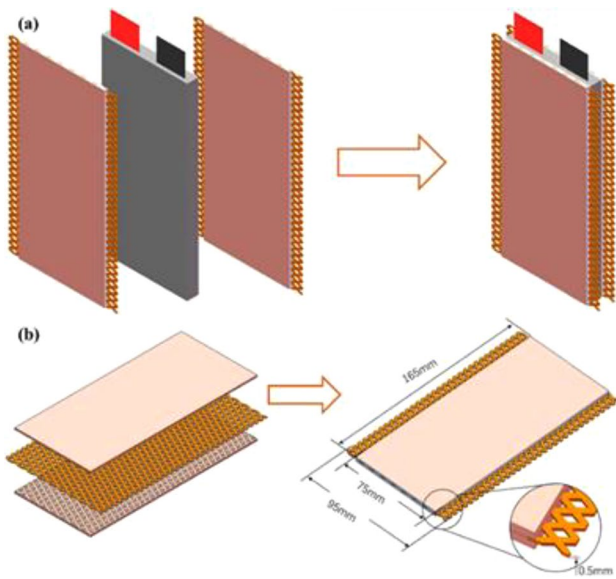


Fig. 32 a Cooling system, and b structure and geometry of the silica cooling plate with copper mesh [72]

By employing liquid cooling strategy to Li ion battery packs, with four mini channels maintains the temperature of the battery pack below 40 °C. Moreover, enhancing performance can be achieved by increasing the number of channels at 1×10^{-3} kg/s. According to Zhao et al. [76], if we increase the amount of water flowing per second, alter the direction of water coolant flow and change the size of channel entrances, we can lower the temperature. However, these adjustments have limitations, in reducing the temperature difference within an area, of below 5 °C.

The numerical investigation of a 5C-discharging prismatic Li-ion power battery fitted with cold plate having mini-channels by Huo et al. [77] suggests that the peak temperature declines with the increase in cooling channel numbers. Among various flow patterns shown in Fig. 35, Design 1 was the most potential in terms of thermal performance, cost, and complexity as in Fig. 36 and adds that for increased ambient of above 25 °C, alternative strategy must be employed as there is high possibility of failure of the system.

Fig. 33 Battery pack and temperature contour for the cells and cooling plates [74]

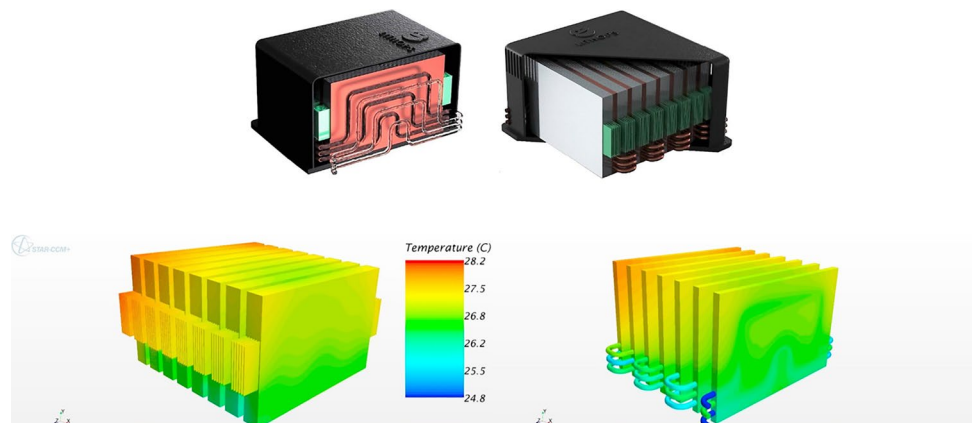
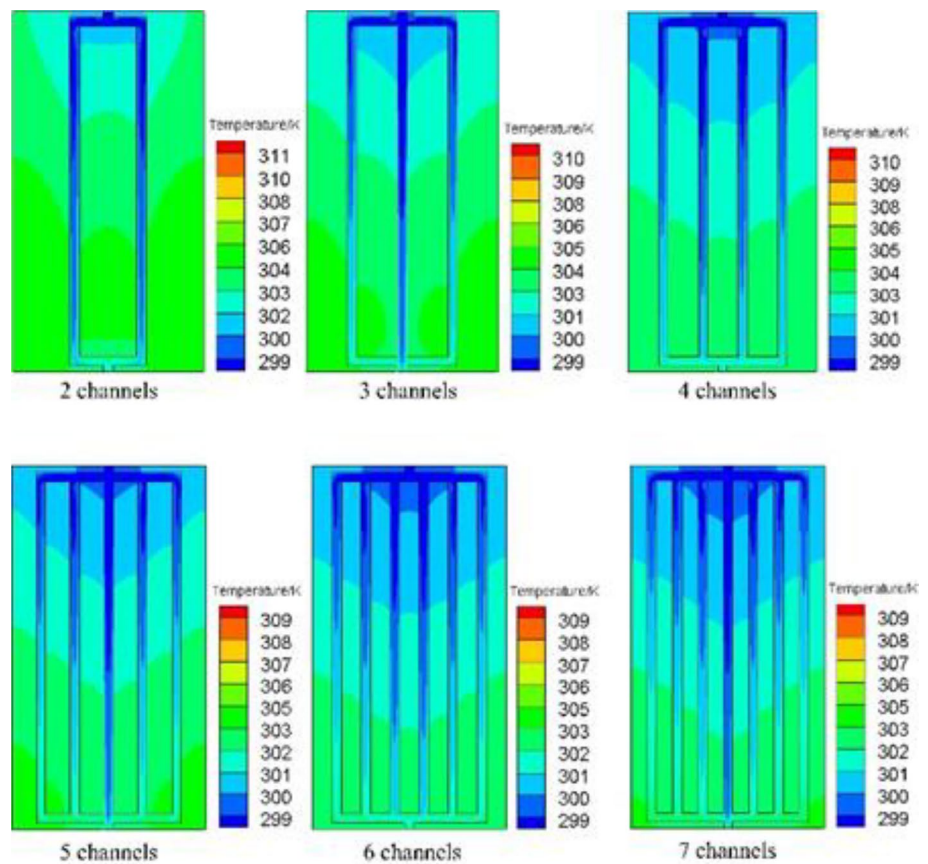


Fig. 34 Temperature fields of different cooling channels in the cold plate [75]



5.2.2 Immersion (or) Direct Liquid Cooling

Liu et al. [78] simulated the immersion cooling of 38,650 cylindrical LIB module using mineral oil by a standard $k-\epsilon$ model at ambient conditions of 25 °C and 101.3 kPa, ignoring the using FLUENT software shown a 18.3% reduction of maximum temperature with the increase in gap between the batteries (1–5 mm) thereby, improving the temperature uniformity when the generation of entropy is

neglected as shown in Fig. 37. The acceleration of the coolant (0–0.35 m/s) declines 63% of the peak temperature but increases the pressure drop up to 342 Pa at a high velocity of 0.35 m/s. The rippling nature of uniform distribution of temperature in the battery pack with the coolant velocity attaining peaks at low velocity and declining at higher velocity led to the optimization of velocity of 0.2 m/s for acceptable temperature difference of 4.66 °C.

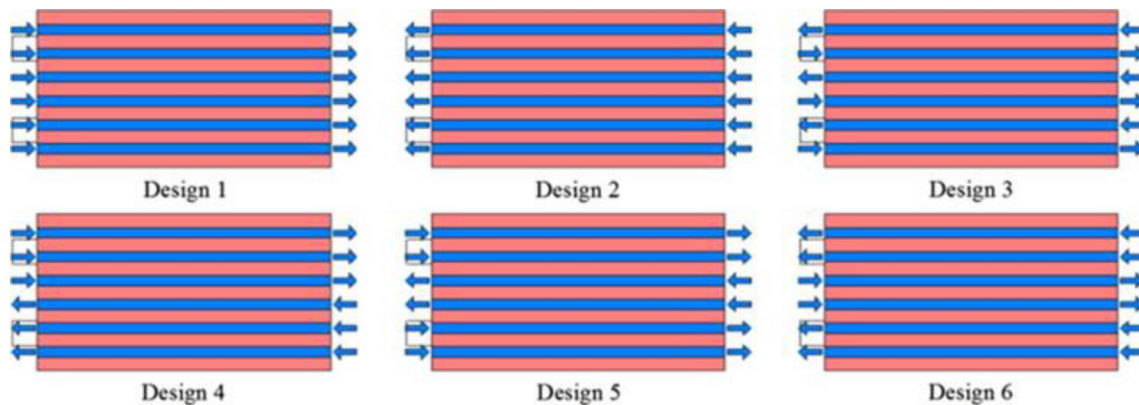


Fig. 35 Schematic of different flow direction [77]

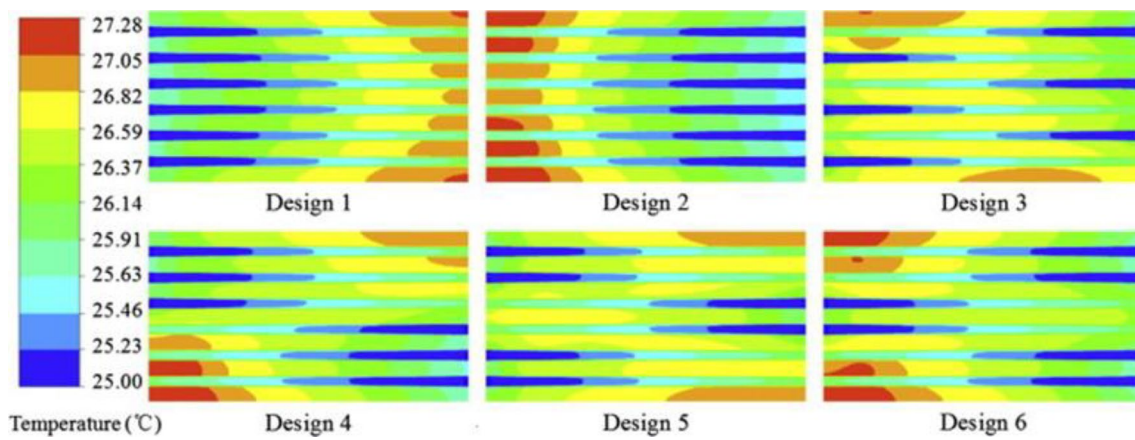
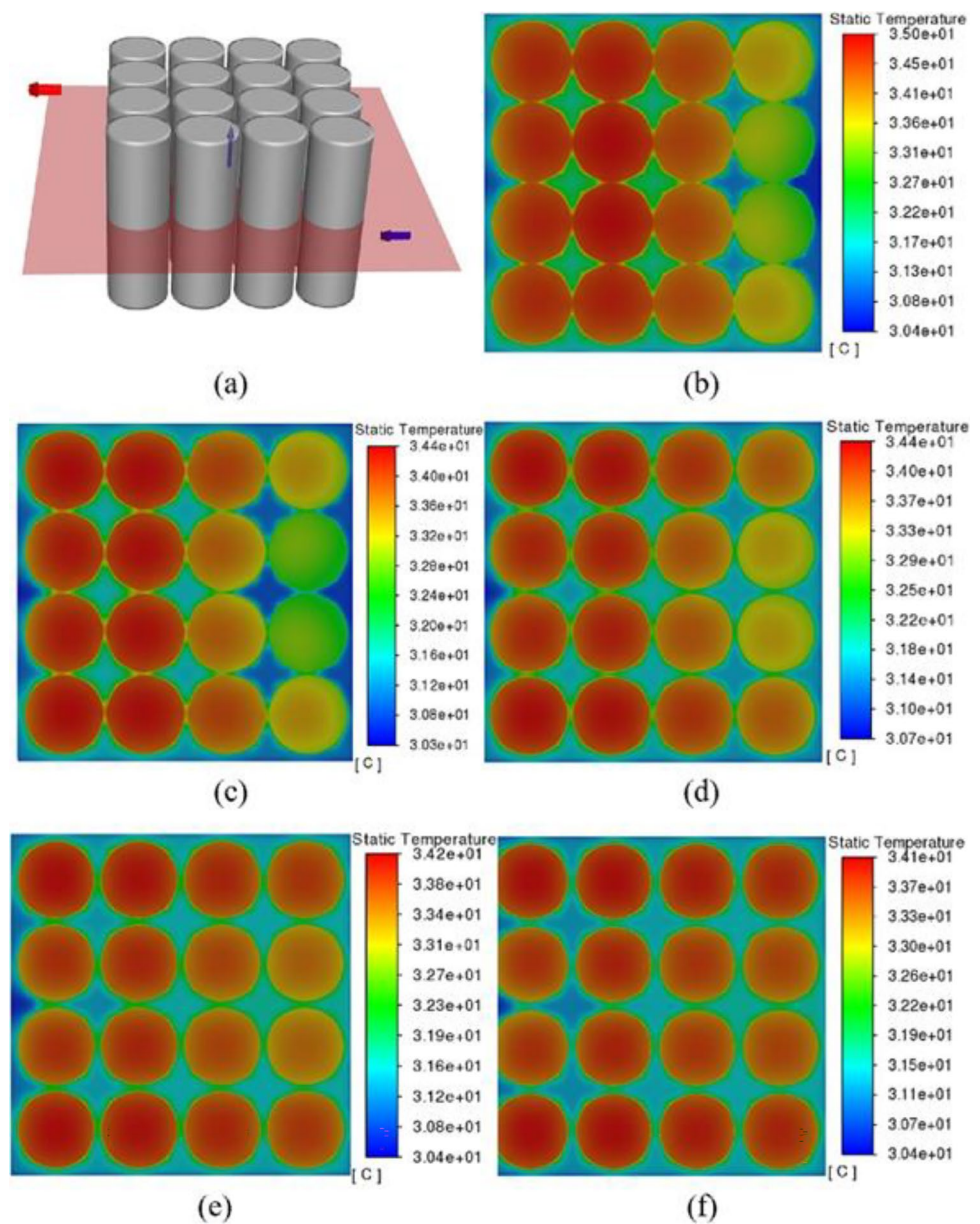


Fig. 36 Temperature distributions for a cold plate with a different flow configuration [77]

Fig. 37 **a** Temperature profile position and **b–f** Temperature contour for battery spacings of 1 mm, 2 mm, 3 mm, 4 mm, 5 mm respectively [78]



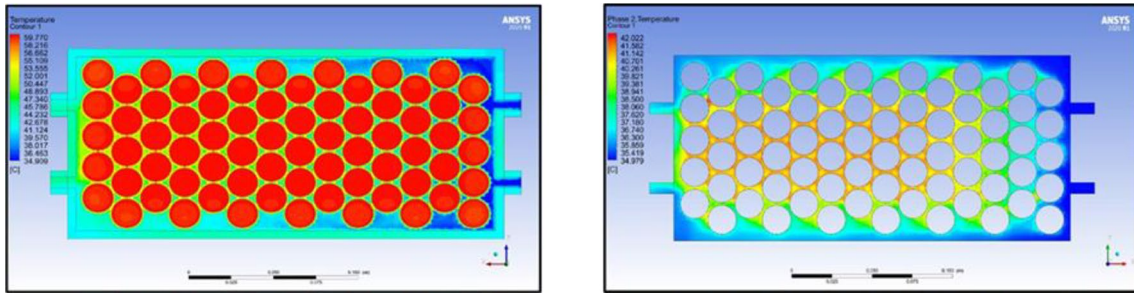


Fig. 38 Battery pack temperature contour without GNP, 0.005 vol% GNP in EG/water [79]

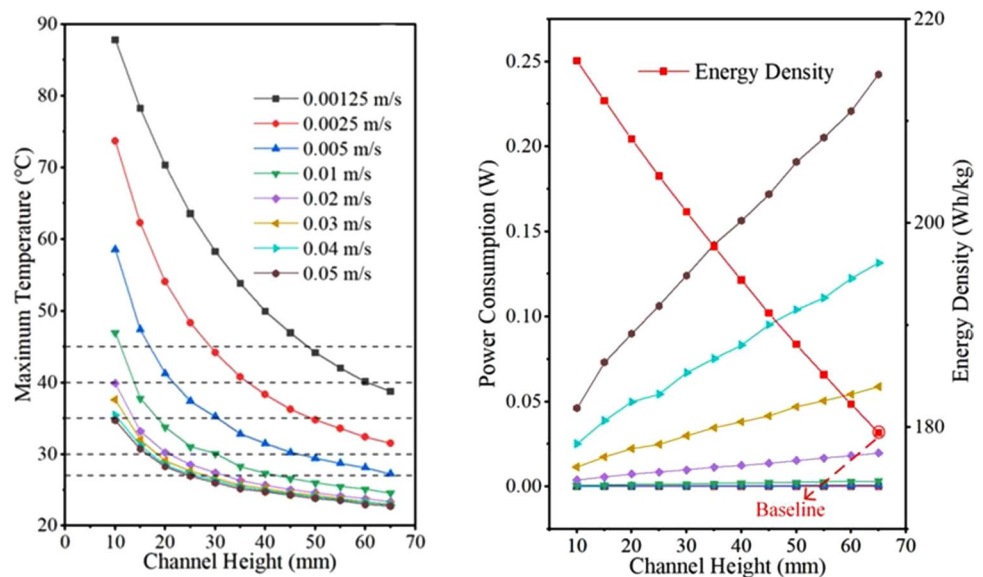
Incorporating amounts of carbon-based nanomaterials of Graphene Nanoplatelets (GNPs) into ethylene glycol and water mixture in equal ratios declined the peak temperature of the Lithium battery pack with Nickel Manganese Cobalt Oxide (NMC) by 24% to 29%. This reduction was achieved through an immersion cooling strategy as demonstrated in Fig. 38. The study conducted by Jindal et al. [79] utilized the SST $k-\omega$ turbulence model along with the energy equation for heat generation. Employed a pressure-based algorithm with a coupled algorithm featuring the PRESTO pressure staggering option, the results showed that as the number of tiers in the battery pack with coolant flow increased there was an increase in heat transfer rate.

Addition of 0.03% phase change material in the form of nano-encapsulate with polyurethane and *n*-nonadecane in the shell and core of the capsule in water by Cao et al. [80] shows a maximum of 13.6% augmented heat transfer. The numerical analysis involves FVM based solver employing SIMPLE algorithm where the Gambit software was employed to discretize the LIB model.

The numerical study of different dielectric fluids including deionized water, mineral oil, and an engineered fluid AmpCool AC-100 at various discharge rates and mass flow rates in a liquid immersion cooling system operating in single phase of the Samsung 26J battery pack by Jithin et al. [81] shows that the dielectric fluid with better thermal properties is more effective and here it was deionized water limiting the increase of temperature to 2.2 °C at the battery discharge of 3C rate with coolant flowing at 0.05 kg/s. The low viscosity of deionized water facilitated in the low power consumption of 0.52 mW. On comparing the mineral oil and AmpCool, the engineered fluid shows 76% less power consumption whereas on highway fuel-economy test, the increase in temperature of 1 °C is limited within the battery pack for all the fluids employed in the study.

In addition to the numerical investigation, Tan et al. [82] studied and optimised the factors for a liquid cooling system, in a fast-charging lithium-ion battery pack. These factors included the speed at which coolant flows the height of the flow path, the number of channel layers and the configuration for cross flow. The researchers found that using a low

Fig. 39 Maximum Temperature and Energy Density of Battery Pack with the power consumption by the cooling system with respect to the height of flow channel [82]



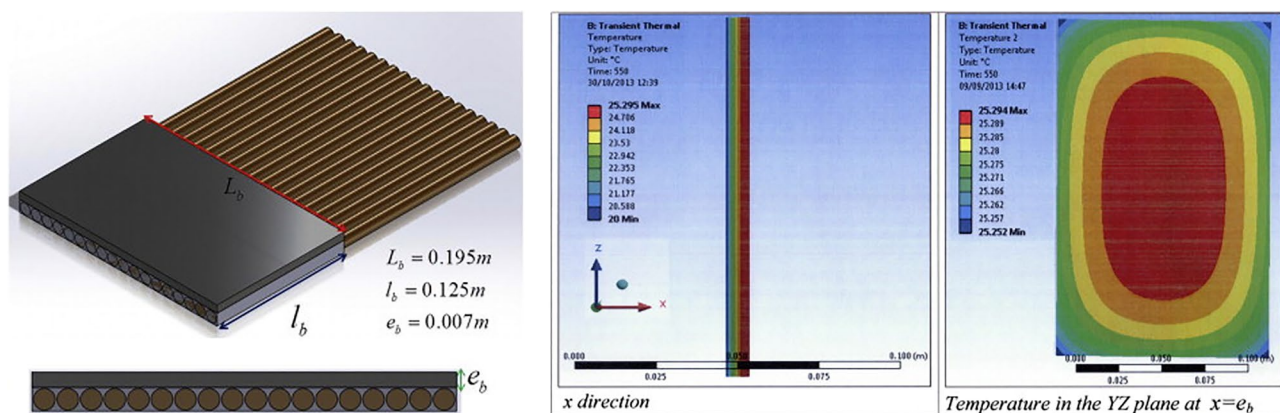


Fig. 40 Design of BTMS with Heat pipe and corresponding temperature contour [89]

height channel and maintaining an optimal coolant velocity can lead to a 20.3% increase in energy density and a 95.3% reduction in power consumption compared to the baseline scenario with a full height channel and an inlet velocity of 0.05 m/s. It is important to note that these improvements were achieved while ensuring that the upper limit temperature requirement was met, as depicted in Fig. 39.

Employment of Al_2O_3 -water nanofluid in the lattice Boltzmann (LB) model BTMS of a Li-ion battery of cylindrical geometry by Huo et al. [83] enhanced the cooling performance by reducing the average temperature with the increase in flow rates and the concentration of nanoparticles in the base fluid but it raised the standard deviation and maximum temperature for the nanofluid having high concentration of nanoparticles.

5.2.3 Heat Pipe Cooling

Heat pipe employed in cooling of the battery pack depicts an maximum increase of 2 °C temperature on the numerical study for a driving cycle of 600 s at a high ambient temperature of 33 °C by Alihosseini et al. [84]. On experimentation showed that the forced cooling of condenser section maintained a constant optimal temperature range even after three cycles in 1C charge and discharge cycles.

The dissipation of heat is facilitated by the Loop Heat Pipe (LHP) of flat structure with graphite sheets employing the coolants of ethanol and water. Bernagozzi et al. [85] simulated the case of fast charging which takes 10 min in the increase of state of charge of the battery from 0.2 to 0.8 resulting 31.5 °C peak temperature which is 3.6 °C better than the standard cooling plate employing ethylene glycol and the addition of graphite sheets maintains the thermal homogeneity of 2 °C within the battery pack with a reduced parasitic power consumption and the need of maintenance.

Wang et al. [86] studied the Micro Heat Pipe Array (MHPA) for heating the battery cell at low temperatures.

On placing a heating pad over the evaporator of the MHPA, an increase in temperature from -30 to 0 °C of the 2-cell module (which has MHPA sandwiched between two cells) is observed in 20 min. In addition, a uniform temperature difference of around 3.03 °C is maintained in the battery pack.

An electro-thermal model of heat pipe is developed in three-dimensions by Kleiner et al. [87] to analyze the thermal performance at an ambient of 30 °C when cooling applied to both the cell and tabs. This approach reduced the temperature by 4.3 °C and effectively maintained temperature homogeneity.

Liang et al. [88] implemented a cooling strategy on a battery pack with five cells with heat pipe of flat shape. On simulated using Simulink and FLUENT, the performance results indicated that relying on free convection conditions for the condenser section is insufficient for maintaining cell temperatures. To achieve this, it is recommended to use water cooling with an estimated heat transfer range of up to 1000 $\text{W}/\text{m}^2\text{K}$ for heat dissipation from the heat pipe condenser.

Greco et al. [89] conducted investigations using a one-dimensional model consisting of 18 cylindrical heat pipes as in Fig. 40 utilizing ammonia as working fluid, with prismatic cells placed between them. A decrease of 23.9 °C in peak temperature is obtained on comparison with forced convection.

Therefore, Li et al. [90] on performing the numerical analysis under thermal run-away conditions concluded that the heat pipes is capable of stopping the spread of troublesome thermal conditions to other batteries of the pack but cannot stop the initiation of such condition.

5.3 PCM Cooled BTMS

Yang et al. [91] numerically investigated the impact of utilizing PCM in a cylindrical battery pack. For different ambient conditions (-20 to 55 °C), it is concluded that the PCM

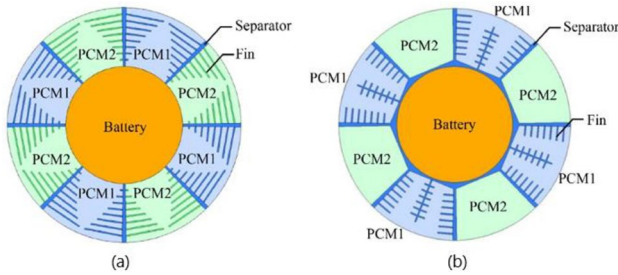


Fig. 41 Schematic of optimization solutions a 1 and b 2 [92]

N-octadecane showed a 20% enhanced performance at 25 °C with the thickness of the PCM being 3 mm.

Li et al. [91] used differently shaped fins with two different phase change materials (PCM 1; pure paraffin and PCM

2; paraffin, with expanded graphite). They investigated the systems performance at various temperatures and discharge rates. The results showed that at 30 °C ambient temperature, the second model having fins in an asymmetric manner reduced the temperature (T_{max}) by 36.15% compared to the unoptimized solution. Similarly at 40 °C ambient temperature the T_{max} reduction was 42.76%. This optimization was achieved through fin reinforced heat transfer technology (Fig. 41).

In the study by Zhang et al. [93] they proposed nine design schemes, for fins in a BTMS that uses paraffin wax as the phase change material (RT-42). These new designs of fins structure as in Fig. 42 aimed to improve heat dissipation by increasing the fin covering area and adding fins as in Fig. 43. The results showed that increasing the fin covering area reduced the cell temperature by 3.14 K while adding

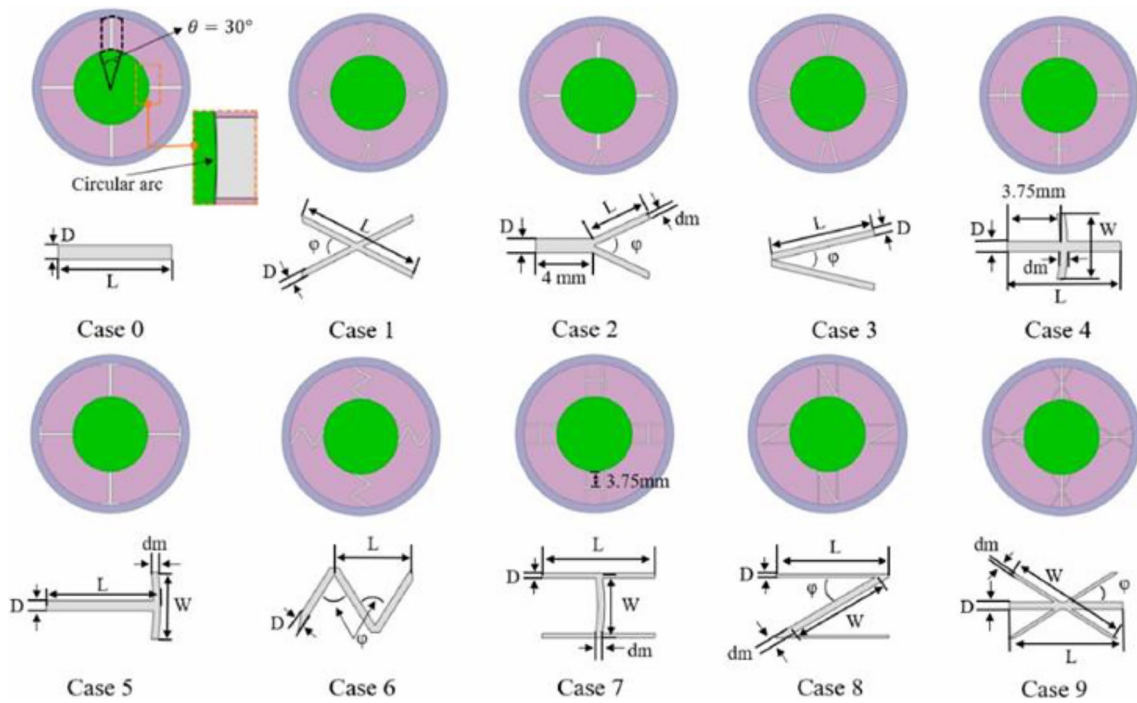


Fig. 42 Fin structure design schematic [93]

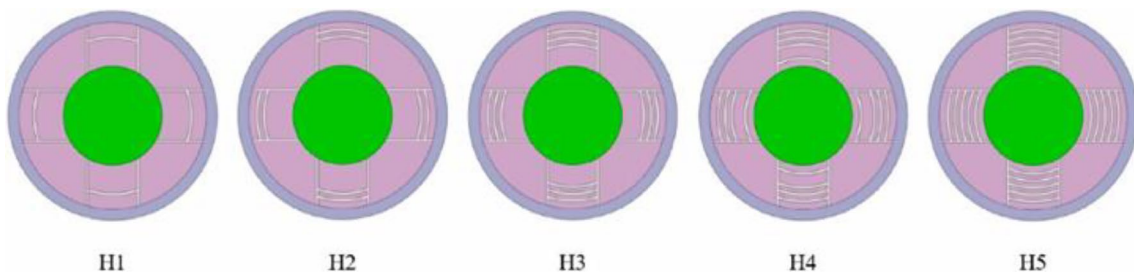


Fig. 43 Schematic diagram of BTMS with different numbers of transverse fins [93]

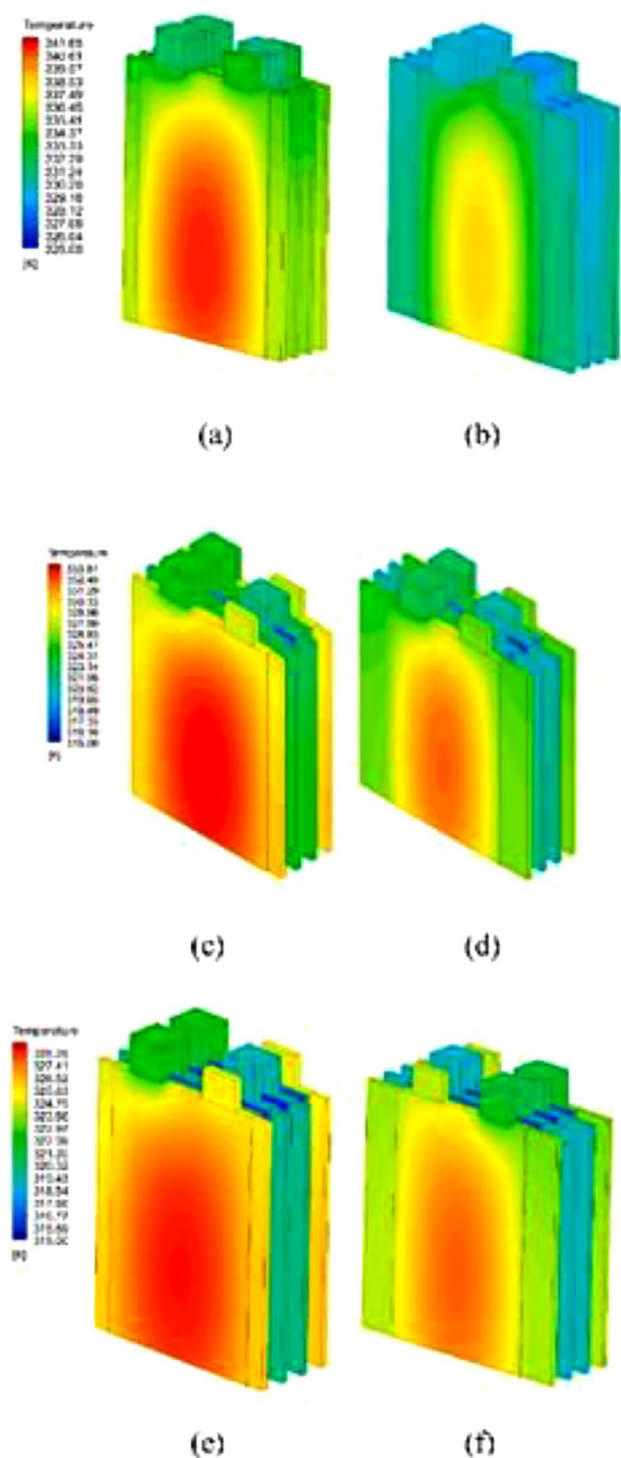


Fig. 44 Temperature Contours at PCM thickness of 7 mm and fin lengths of **a** 14 mm, **b** 30 mm; and **c**, **d** with 9 mm thick PCM; and **e**, **f** with 12 mm thick PCM [94]

transverse fins further decreased it by 3.92 K. However, in high temperature scenarios extending the arc length of transverse fins adversely affected system thermal performance while increasing their thickness decreased heat storage

capacity. The fins of case 7 H6 were designed to maintain a cell temperature of 318.15 K resulting in a 14.98% improvement, in heat transfer capability. This allowed for an increased operating time of 131.5% and a reduced system weight of 10.28%.

Different Phase change material thickness with varying lengths of aluminum rectangular fins introduced by Verma et al. [94] employing lauric acid showed that using 30 mm fins resulted in a significant temperature drop ranging from 16 to 26 K with PCM thicknesses between 7 and 12 mm as in Fig. 44b, d, f being optimal when the batteries were exposed to temperatures of 40 °C. However, the inclusion of both PCM and fins adds weight to the EVs chassis leaving room for research on finding an optimum PCM thickness.

Jilte et al. [95] numerically studied the BTMS using two-layer nano-enhanced PCM (nePCM) which results in maintaining optimal temperature in the battery pack by limiting the rise of temperature within 6 °C is obtained on arranging the PCMs in multiple layers in radially transverse manner. The performance was comparatively lower when the layers of PCMs are axially arranged.

The introduction of fins in the PCM matrix forms a thermal conductive network in longitudinal direction with the cylindrical rings in a dimensionless radial distance of 0.2 between the cylindrical ring and battery enhances the thermal performance whereas Multiple ring usage increases battery-PCM heat transfer area, but negatively impacts BTMS thermal management performance due to PCM reduction concludes Sun et al. [96]. Battery working time increases with longitudinal fin number, enlarging thermally conductive network, and shortening due to PCM reduction for fin numbers above 8 in BTMS as in Fig. 45. This PCM-Fin strategy is efficient even at a heat load of 20 W.

The fusion of different volumes of copper foam with phase change material particularly pure paraffin numerically evaluated by Ranjbaran et al. [97] showcased that copper foam has significant influence on the fraction of liquid and life time of PCM as in Fig. 46 revealing lower liquid fraction at low volume concentration (1–6%) of copper foam such that increasing the lifetime of the phase change material whereas, with high concentration of copper foam the liquid fraction of PCM evidently rises over 85%, lowering the capability of PCM to absorb the heat and becoming ineffective. A concentration of 6% copper foam with 15 mm thick phase change material is concluded as optimal.

Verma et al. [98] investigated the phase change material, in specific Capric acid [$\text{CH}_3(\text{CH}_2)_{2n}\text{COOH}$, a fatty acid], for its thermal performance under different operating conditions. A numerical comparison with the conventional paraffin reported that 9 mm thick paraffin brings the temperature down to 308 K from 312 K whereas the temperature was made 305 K with Capric acid of 3 mm thick at the conditions of 294 K ambient and a rate of 6870 W/m³ heat generation.

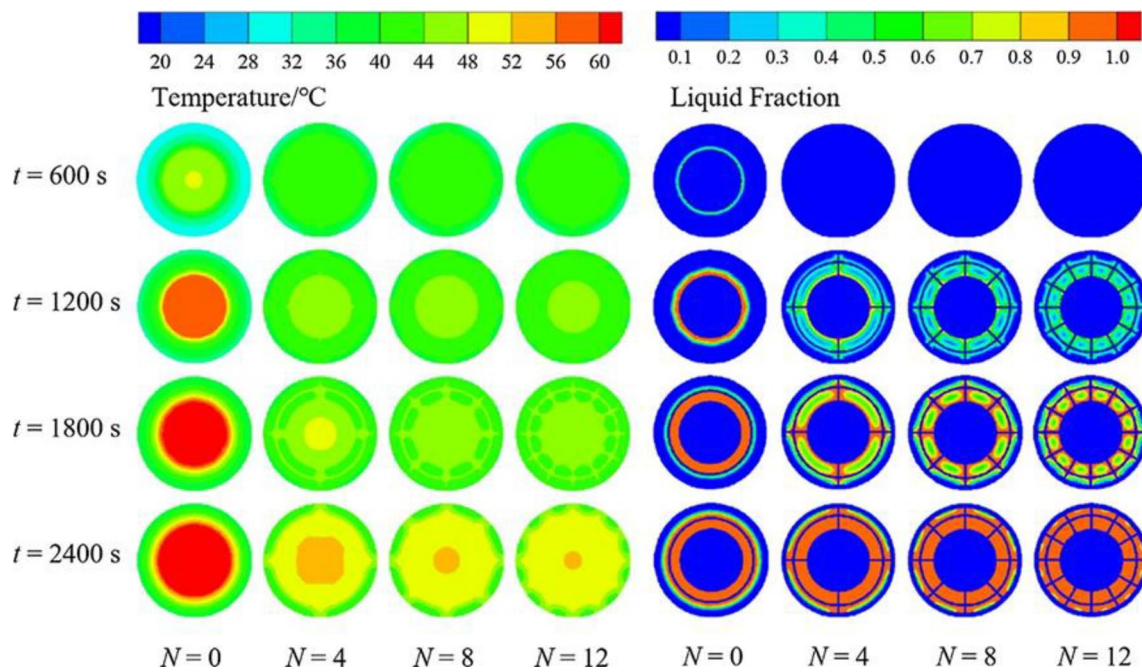


Fig. 45 The temperature and fraction of liquid contours of the cooling strategy with varying number of longitudinal fins [96]

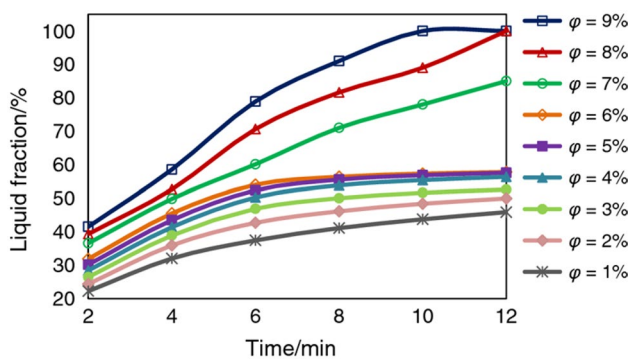


Fig. 46 Influence of different volume copper foam on the liquid fractions of PCM [97]

The PCM became inefficient for the higher rates of 63,970 W/m³ during discharge, 323 K ambient, and needs to be coupled with other cooling systems as the temperature shoots up to 342 K which is very fatal.

Al-Zareer et al. [99] employed a phase change cooling strategy in prismatic battery using propane whose latent heat of vaporization is effectively utilized in the cooling strategy as in Fig. 47. On solving using COMSOL with propane of 8.5 bar saturation pressure and 35 °C ambient conditions, it was reported that the battery pack is maintained at a maximum temperature of 49 °C even at high discharge rate of 6C with 15% propane pool. And 5% of this propane pool is covered on the front surface of the battery with 4C discharge rate.

To understand the behaviour of a cylindrical battery cell, Greco et al. [100] examined a simplified one-dimensional model using phase change material combined with compressed expanded natural graphite (CENG). This analytical/computational model produced results that closely matched those obtained through 3D simulations using SALOME.7.4/SYRTHES.4 software. The study revealed that employing PCM/CENG cooling techniques kept the temperature below 40 °C for 2.9 h reducing it from an initial value of 75 °C to, around 45.9 °C. However, it should be noted that there was still a temperature gradient exceeding 10 °C within the battery. The study also focused on investigating the influence of density, thermal conductivity and porosity of PCM/CENG. It was found that there is an impact up to a limit, beyond which no further effect is observed.

With the increase in the phase change material thickness from 3 to 12 mm reports a reduction of temperature of the battery pack from 2.8 to 3 K on the numerical study by Javani et al. [101] using ANSYS FLUENT as in Fig. 48 under transient conditions and a 10% improvement on the temperature distribution is also added at the initial conditions of 294.15 K and 3 mm-thick PCM, which is crucial for electric vehicle thermal management systems.

5.4 Hybrid Cooling System

Choi et al. [102] numerically studied a hybrid cooling structure combining immersion cooling strategy

Fig. 47 Schematic of the battery pack design employing propane [99]

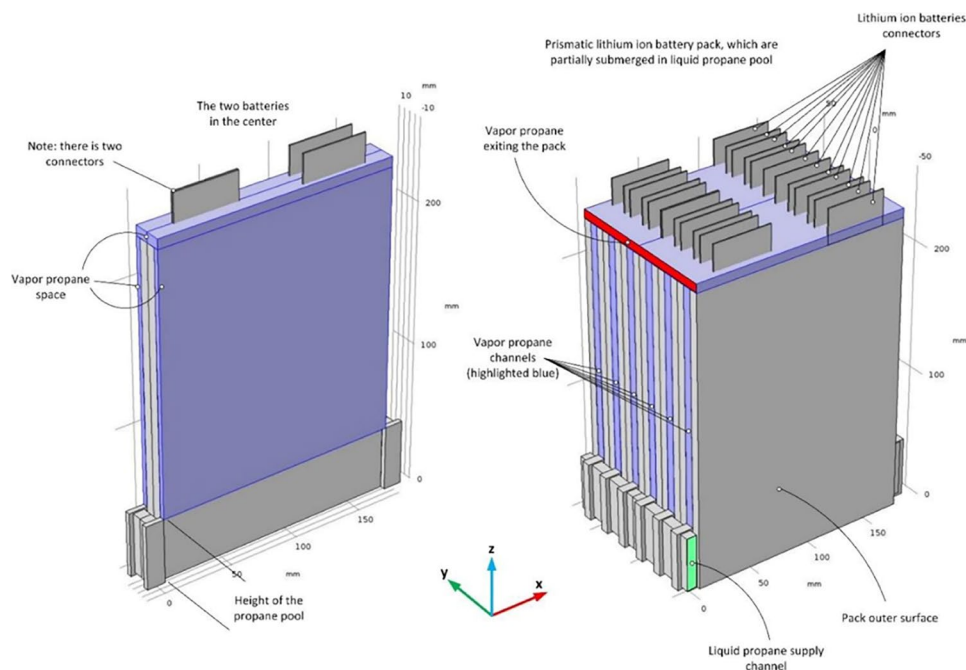
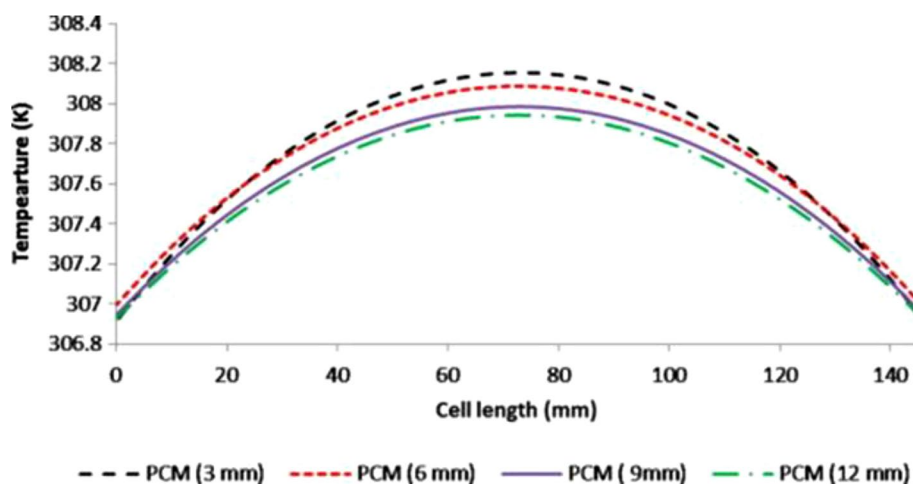


Fig. 48 Distribution of temperature along the cell length for varying PCM thickness [101]



(hydrofluoroether Novec 7500) with pass partition and graphite fins in lithium nickel manganese cobalt pouch-type battery as in Fig. 49 using ANSYS FLUENT software. Cell level evaluation emphasized the advantage of hydrofluoroether over other dielectric fluids. The effect of gravity in the distribution of fluid depicts upward flow provides more effective cooling as in Fig. 50. Further simulation of a 40 celled module, resulted a 45.4% and 61.0% reduced pressure drop and power consumption when pass partition is employed with fins of graphite material providing a homogeneous temperature distribution as in Fig. 51.

Chen et al. [103] integrated the forced air-cooling strategy with the composite PCM reducing the module temperature by 15.9 K at 5C discharge rate on numerical investigation and the active cooling strategy is eminent and efficient than

the PCM at low discharge rate. As the thickness of PCM is increased as in Fig. 52, the lowering of peak temperature is restrained with certain thickness. The fusion of graphite to the PCM in a small amount of 4.6 wt% can drastically improve the heat absorption capacity of PCM.

Mousavi et al. [104] numerically investigated the prismatic batteries sandwiched between vertical cold plates of mini-channels and horizontal plates of PCM as in Fig. 53 showing a maximum reduction in temperature of up to 16.64 K when 3 PCM plates are employed and temperature difference is reduced by 16–33% on varying the water velocity in mini channels as in Fig. 54 for discharge rates of 3C. The energy required for pumping the coolant in the cold plate is 45 and 68% lower for the hybrid strategy including

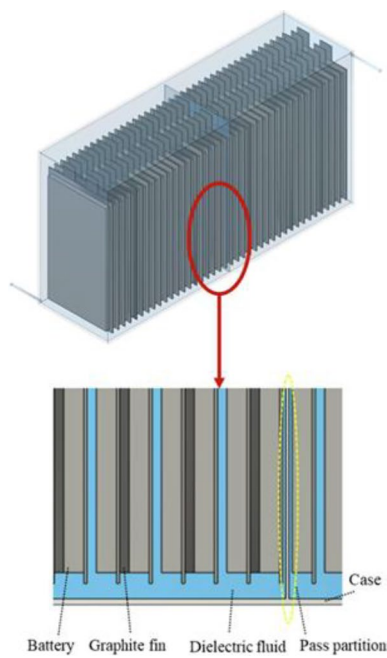


Fig. 49 Schematic of direct cooling with pass partition combined with graphite fin [102]

1 and 3 PCM plate systems, compared to the case without PCM for similar thermal performances.

Hybrid strategy with cold plate for a Li-ion module battery cell at 5C discharge rate used in BMW i3 and Volkswagen commercial EVs with different microchannel types as shown in Fig. 55 on numerical investigation by Rabiei et al. [105] concludes wavy channel reduces the maximum temperature but fails in maintaining temperature uniformity, aluminum foam results lowest maximum temperature

but consumes highest power of up to 29 mW for 0.3 m/s. On design aspects, the wave of the channels is varied to an amplitude of 50 and 75 μm in cases 2 and 3, and the thickness of 0.46 porous aluminum metal foam is of 50 and 100 μm , in cases 5 and 6 respectively. Thereby hybrid system with metal foam and a micro cooling channel of cases 5 and 6 is efficient with 95% reduced parasitic power consumption compared to case 4.

Angani et al. [106] combined two active cooling strategies of liquid cooling using parallel pipe and air-cooling strategy with fan. The peak temperature was maintained at 31.9 °C with a temperature deviation less than 1.4 °C at discharge conditions of 1C rate. On comparing with conventional cooling strategy of using cold plate with Zig Zag channels fixed at bottom, the hybrid system suggested, depicts a 28% improvement in thermal performance.

The combination of Paraffin matrix with liquid cooling strategy shown an improved cooling performance along with the segmented PCM matrix design on addition of expanded Graphite contents (0–12%). The cooling performance is also impacted by varying the length of segments which increases the space (L) up to 24 mm between the cells and the diameter of the channel (d) from 2 to 5 mm at 4C discharge rate. In addition, Xing et al. [107] efficiently used the PCM matrix by delaying the cooling effect of liquid coolant, which in turn reduces 33.3% power consumption.

The cooling strategy employing cold plates maintained a difference of 3.66 °C in the prismatic battery pack and Zeng et al. [108] combined a micro heat pipe array (MHPA) which is of U shape with the above strategy reducing the temperature deviation further to 0.66 °C and 2.16 °C at 1C and 3C discharge conditions and resulting in 34.11% reduction in T_{max} at 1C. By using a combination of the Nondominated

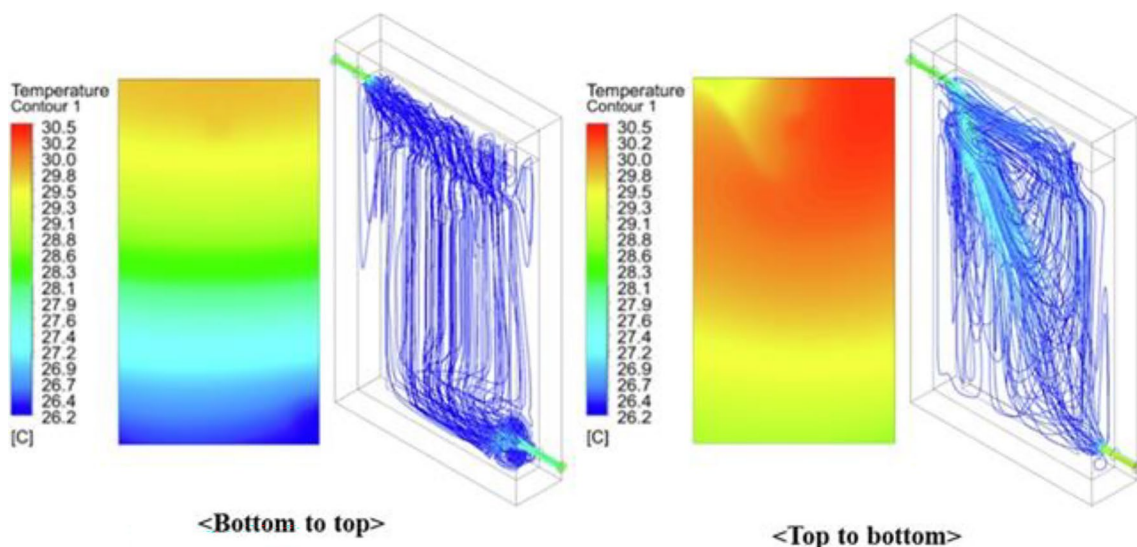


Fig. 50 Temperature distribution and streamlines for different flow direction [102]

Fig. 51 Temperature distributions for baseline and hybrid strategy [102]

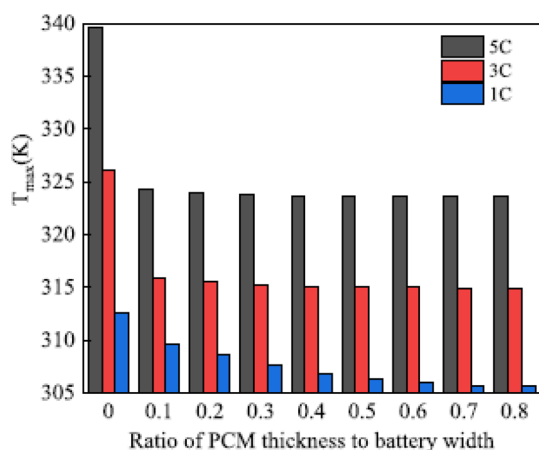
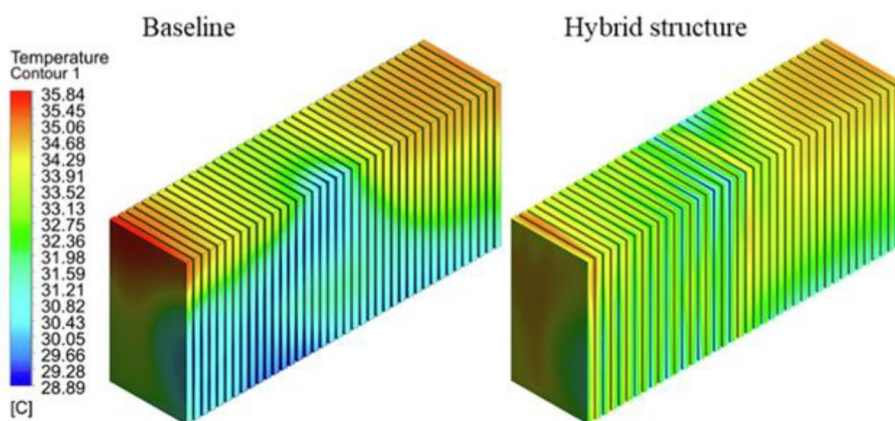


Fig. 52 PCM thickness effect on the battery peak temperature [103]

Sorting Genetic Algorithm II (NSGA II) and the Response Surface Methodology (RSM) optimized the system to increase the energy density by 13.75%.

Hekmat et al. [109] on integrating the cooling channels with the PCM as shown in Fig. 56 achieved a homogeneous temperature distribution in prismatic cells. The researchers add that the mean temperature of the module is not affected by varying the flow directions in the channels but a better homogeneity is maintained in BTMS 3 having counter flow channels having reduced temperature difference of 2.8 K when water coolant is flowing at 0.0125 m/s for 2C discharge rate as in Fig. 57.

Shahid et al. [110] numerically simulated a hybrid cooling systems combining air and liquid cooling using the $k-\omega$ Shear Stress Transport (SST) model and the volume of fluid (VOF) multiphase model in ANSYS FLUENT resulting a 50% improvement in reducing the increase of maximum temperature in Concept-2 where fiber channels of hydrophilic nature is introduced between the cells which makes the cooling evaporative in nature compared to Concept-1 integrating liquid jackets with turbulence boosting vortex

generators and jet inlets. But homogeneous temperature distribution is better in 1 than 2 as Fig. 58 because of the direct contact of liquid constrained in liquid jacket with the cells' surfaces and turbulent mixing of air. It is concluded that Concept-2 has better thermal performance than 1 and is advantageous in terms of safety neglecting the leakage issue.

A combination of PCM with the cooling plate strategy enhanced the cooling performance when solved by Akbarzadeh et al. [111] under a real driving cycle using the $k-\epsilon$ model of ANSYS FLUENT software using a pressure-based solver. From Fig. 59, it is clear that the temperature homogeneity is better in the hybrid strategy and 25% pumping power is also conserved. The module with hybrid strategy reduces the energy required for warming the battery under cold conditions by maintaining a temperature of 5.5 °C more than the conventional cooling plate.

Li et al. [112] linked a passive strategy of heat pipes with active cooling plate for prismatic cells as in Fig. 60. By employing Volume of fluid (VOF) model and $k-\epsilon$ model of ANSYS FLUENT for heat pipes and cold plate respectively for numerical investigation, an eminent decrease in peak temperature and difference in temperature is resulted and the obtained results are further optimised with the orthogonal design of experiment on the geometry of the cooling channel with the objective of minimum peak temperature and temperature difference of the battery module.

Flat heat pipes and PCM cooling strategy coupled to form a hybrid cooling strategy by Karimi et al. [113] is investigated numerically using COMSOL Multiphysics software where Autodesk Inventor software is employed for CAD, considering the generalized heat source equation. The results clearly depicts that the hybrid strategy is superior to solely operated heat pipes as the hybrid system lowers the temperature to 35.8 °C whereas the heat pipe maintains a temperature of 46.8 °C.

Safdari et al. [114] coupled the air-cooling strategy with PCM and investigated the various PCM encapsulation configurations of circular, rectangular, and hexagonal

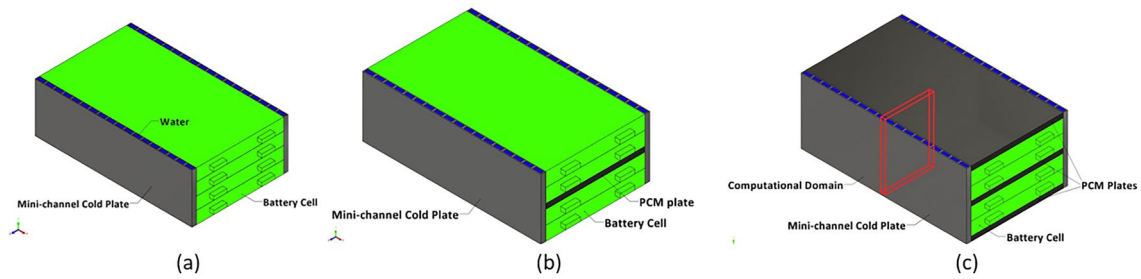
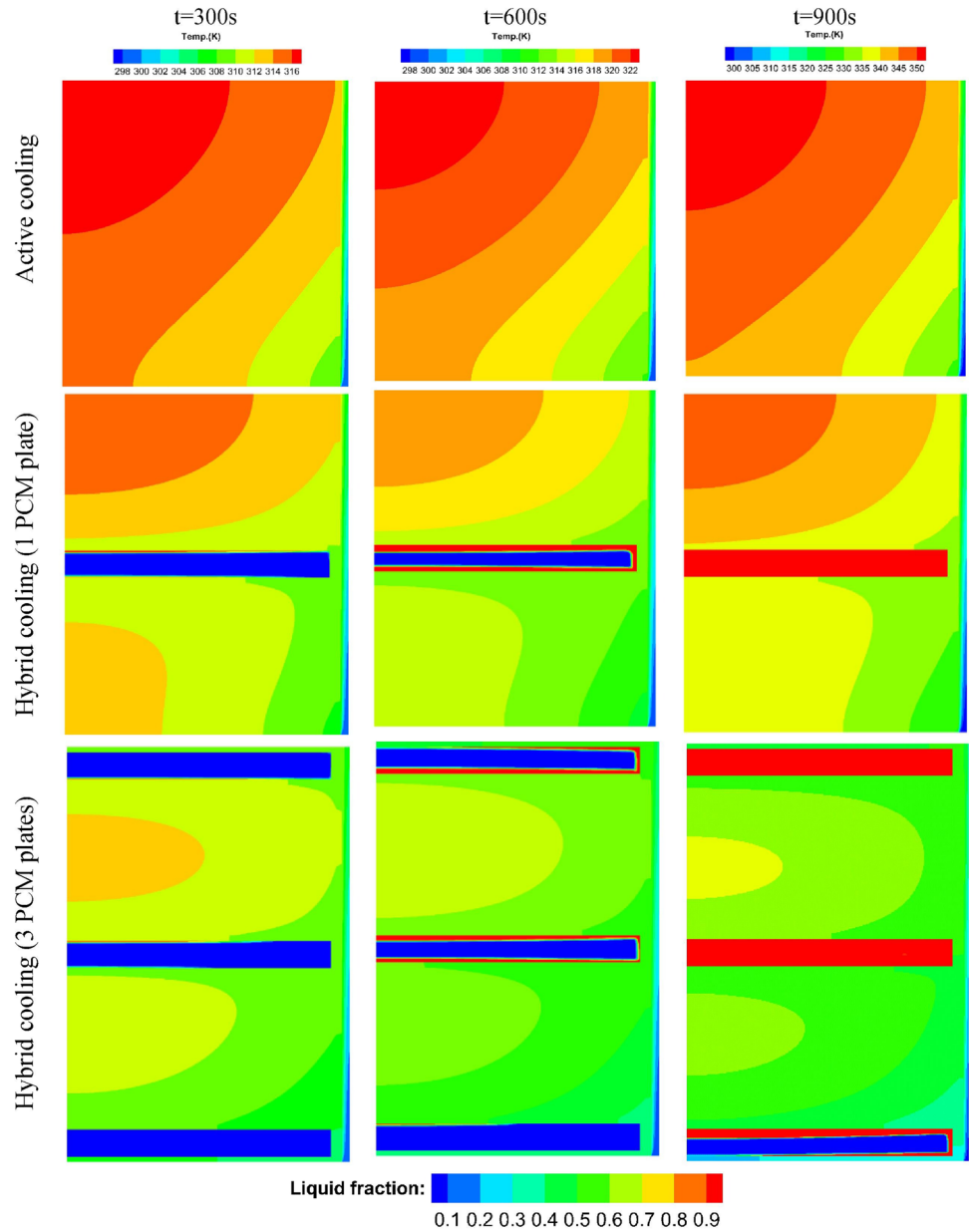


Fig. 53 A part of the battery pack having cooling strategy **a** without PCM plates, **b** with 1 PCM plate, and **c** with 3 PCM plates [104]

Fig. 54 Contours of battery temperature and melting rate of PCM at 3C rate [104]



cross-section with the finite volume method using FLU-ENT which is discretised by Gambit software. Among

these configurations, a relatively lower mean temperature is depicted in the rectangular form as the channels uniformly

Fig. 55 The schematic of different channel design with metal foam [105]

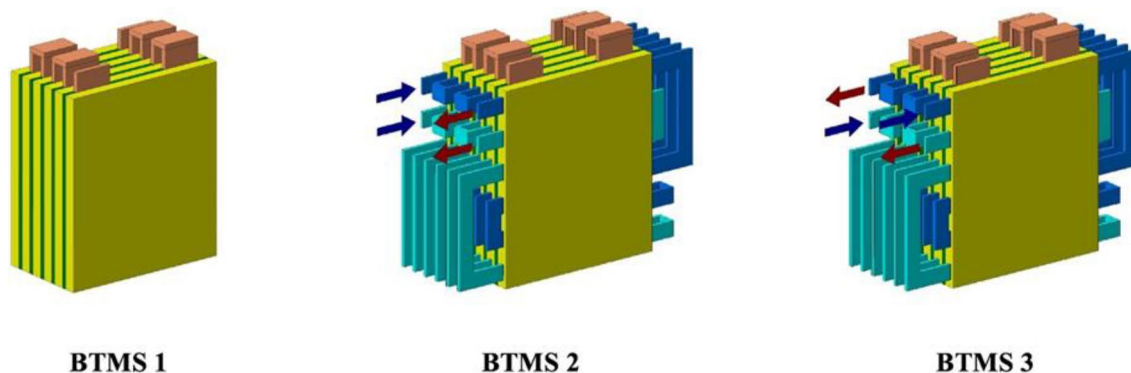
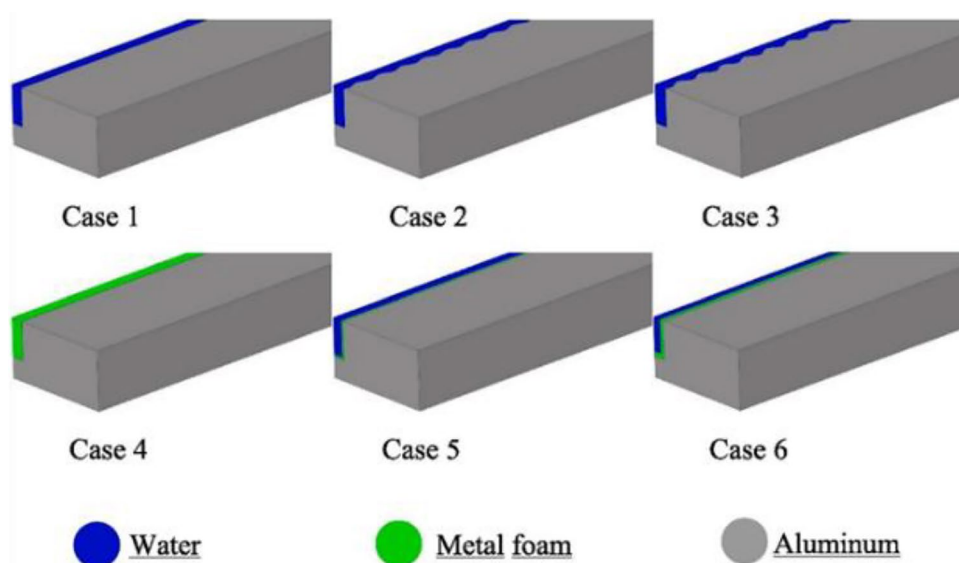


Fig. 56 Schematic of BTMS 1 (PCM only), BTMS 2 (hybrid with parallel flow channels), and BTMS 3 (hybrid with counter-flow channels) [109]

distributes the air in the module with rectangular encapsulation. The cooling effect can further enhance up to 64% when force convection of air is introduced with a velocity of 0.2 m/s air flow.

Behi et al. [115] predicted the hybrid system combining air cooling and heat pipes with copper sheets (HPCS) for a cylindrical celled battery module as in Fig. 61 which lowered the peak temperature to 37.1 °C which is 42.7% better than natural air cooling and improved temperature homogeneity by 73.4% using COMSOL Multiphysics® software at an optimized cell spacing of 2 mm with 2 m/s air velocity, and 26 °C ambient temperature.

Gan et al. [116] numerically investigated heat pipes combined with wave-shaped aluminium sleeves and cooling plates. The researcher enhances the thermal performance by extending the condenser portion of the heat pipe such that the coolant attains the subcooled state thereby the coolant can effectively cool the battery. Addition of aluminium

sleeves with varying heights to battery cells, in various locations not only enhances temperature uniformity within the system but also reduces its overall weight when compared to using sleeves of identical heights as in Fig. 62.

Zhang et al. [117] numerically investigated the BTMS combining flat heat pipes using acetone as the coolant with fins as in Fig. 63 for prismatic LiFePO₄ power batteries using STAR CCM+ software. On comparing with natural convection and aluminium plates cooling strategy at 2C discharge rate and 25 °C ambient, the hybrid strategy depicted a 81.0% and 44.3% reduced maximum temperature rise, and 73.7% and 50.1% homogeneous temperature distribution respectively. However, at the high discharge rate of 8C, the proposed model failed to maintain the temperature difference within the limits.

Experimental and numerical study of a BTMS that integrates PCM with air cooling by Xie et al. [118] employing CAD software SolidWorks and ICFM CFD simulation

Fig. 57 Temperature distribution contours under 2C discharge rate: **a** BTMS 2 and **b** BTMS 3 [109]

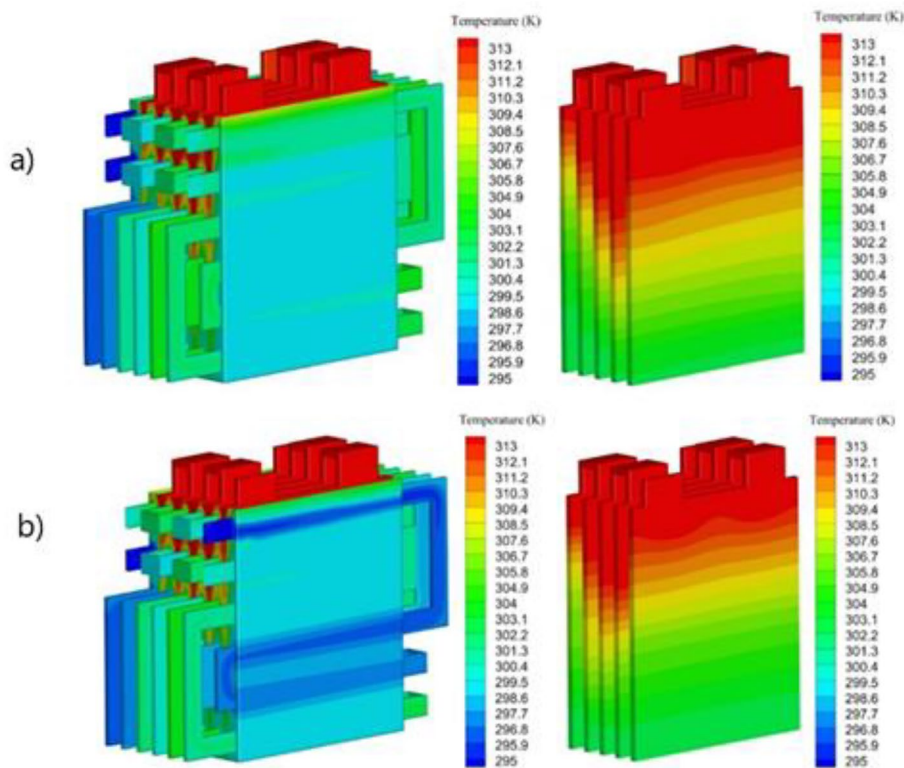
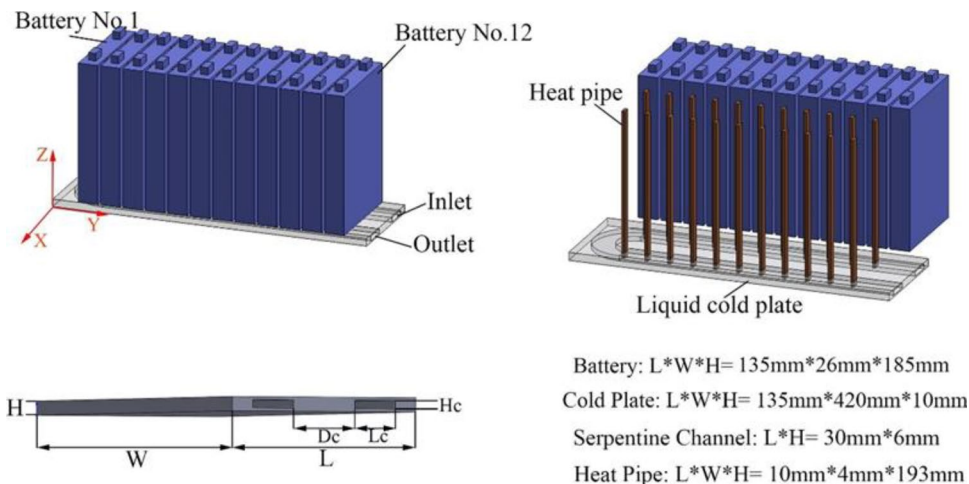


Fig. 58 Temperature distribution in **a** Concept-1 and **b** Concept-2 [110]



software resulted an efficient control in the increase of battery pack temperature when air cooling strategy is employed in 4C charge–discharge cycles at flow rates exceeding 300 m³/h, while integrated systems achieve good thermal management with a 100 m³/h air flow rate. With no additional battery power consumption, the peak temperature of the battery pack was maintained at 49.2 °C with the aid of this integrated system and withstands up to 6 cycles.

Rao et al. [119] numerically simulated the cooling system combining Aluminium PCM coolant with cooling channels using ANSYS FLUENT as in Fig. 64a, b where the effects of radiation and the contact resistances are neglected. The

results that the increase in channels increases the performance of the strategy and the performance was peak with 8 channels when the coolant flows at 8×10^{-4} kg/s as in Fig. 65.

5.5 Other Cooling BTMS

There are methods of cooling battery cells at target areas, such as the welding zones and electrode tabs. One of these methods is tab cooling. Research suggests that the thermal resistance between current collectors and electrodes cannot be neglected due to the welding connection resistances

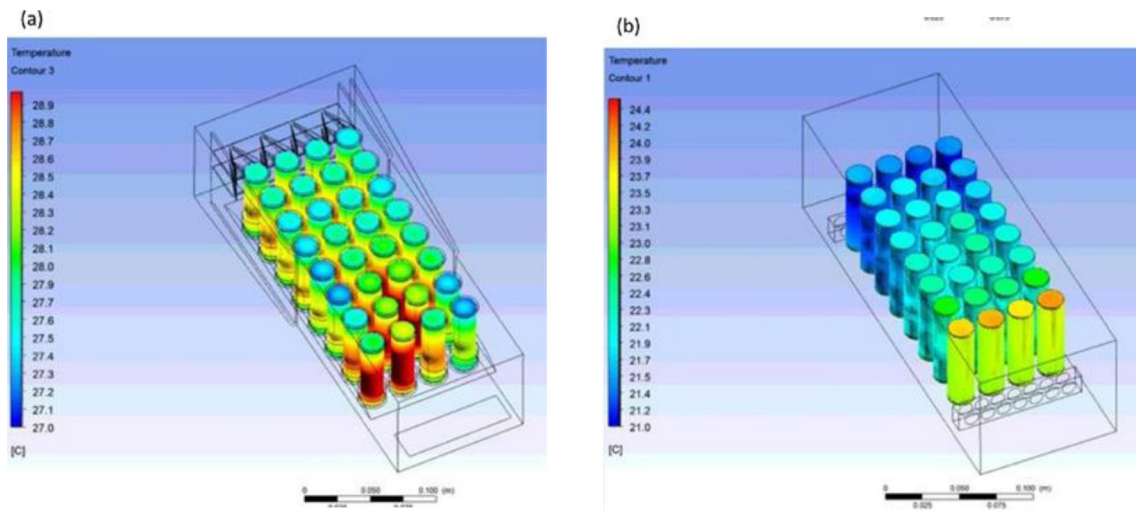


Fig. 59 Schematic of the hybrid strategy with the temperature contours [111]

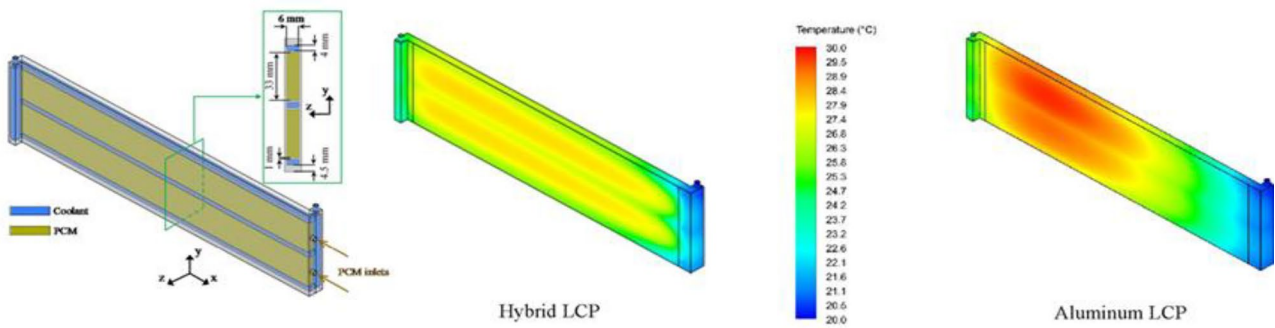


Fig. 60 Schematic of the liquid cold plate coupled with heat pipes [112]

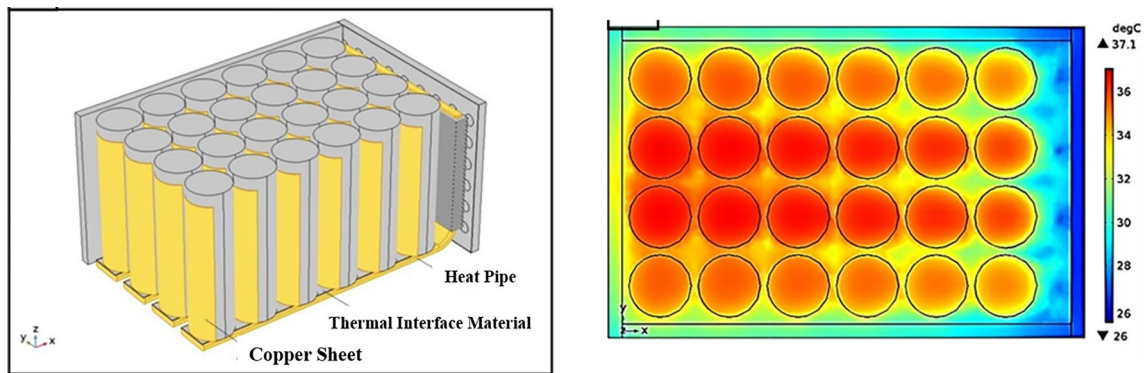


Fig. 61 Schematic illustration and temperature contour of battery module with HPCS [115]

[120]. As a result, the surface cooling method tends to cause heterogeneous distributions of temperature within the regions of battery leading to more severe fade in the capacity. On the other hand, tab cooling provides uniform thermal performance [121]. The choice between tab and surface

cooling depends on factors like desired lifetime and balance between capacity fading and output performance [122].

Evaporative cooling is an emerging technology used in management systems due to its capability of dissipating the heat flux at a reasonable cost. In this method coolant droplets

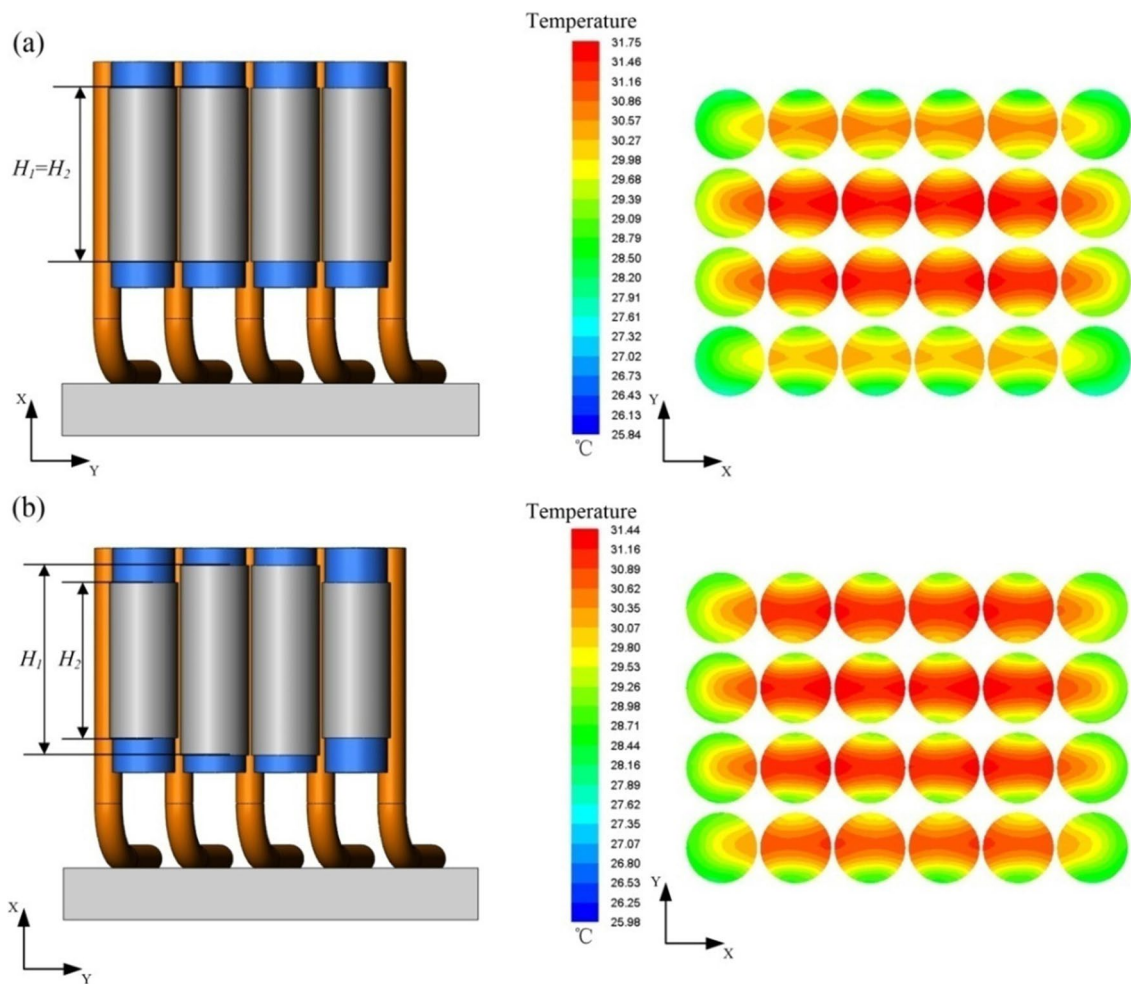


Fig. 62 Side view of the BTMS with top view battery temperature counters: **a** aluminium sleeves with the same heights and **b** aluminium sleeves with different heights [116]

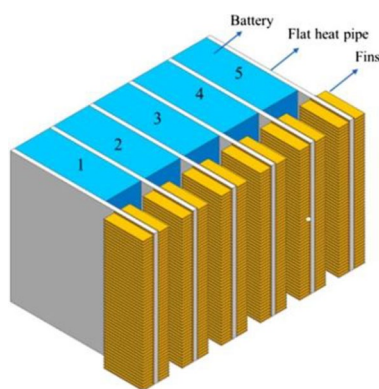


Fig. 63 Physical model of the cooling system combining flat heat pipes and fins [117]

absorb heat from surfaces resulting in evaporation and providing effective cooling. The main advantage of cooling is that it does not require equipment, like pumps, cold plates or

heat exchangers commonly found in traditional liquid cooling systems. Among the evaporative cooling strategy mist cooling and spray cooling techniques are employed in the battery thermal management systems (BTMS) for enhancing heat transfer [123, 124].

In their study, Yang et al. [125] conducted an analysis on water spray evaporation integrated with air cooling strategy, within a six celled battery pack. They developed a three-dimensional model comprising multiple nozzles positioned in front of the airflow direction. By spraying water from these nozzles, it dispersed into droplets that are collectively conical in form. The tiny droplets move along with the airflow and evaporate which leads to a decrease in the air temperature. This in turn increases the temperature difference, between the battery and the surrounding air effectively dissipating the heat generated by the battery. The effective drop in the peak temperature using spray cooling is evident as in Fig. 65 compared to dry cooling.

Fig. 64 **a** Coupling of PCM and mini channels [119]. **b** Varying thermal behaviour with the number of channels [119]

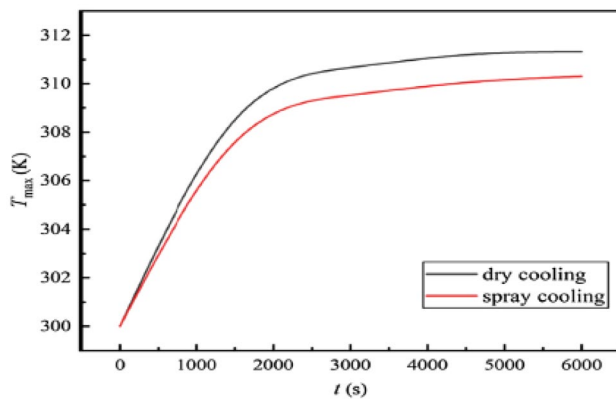
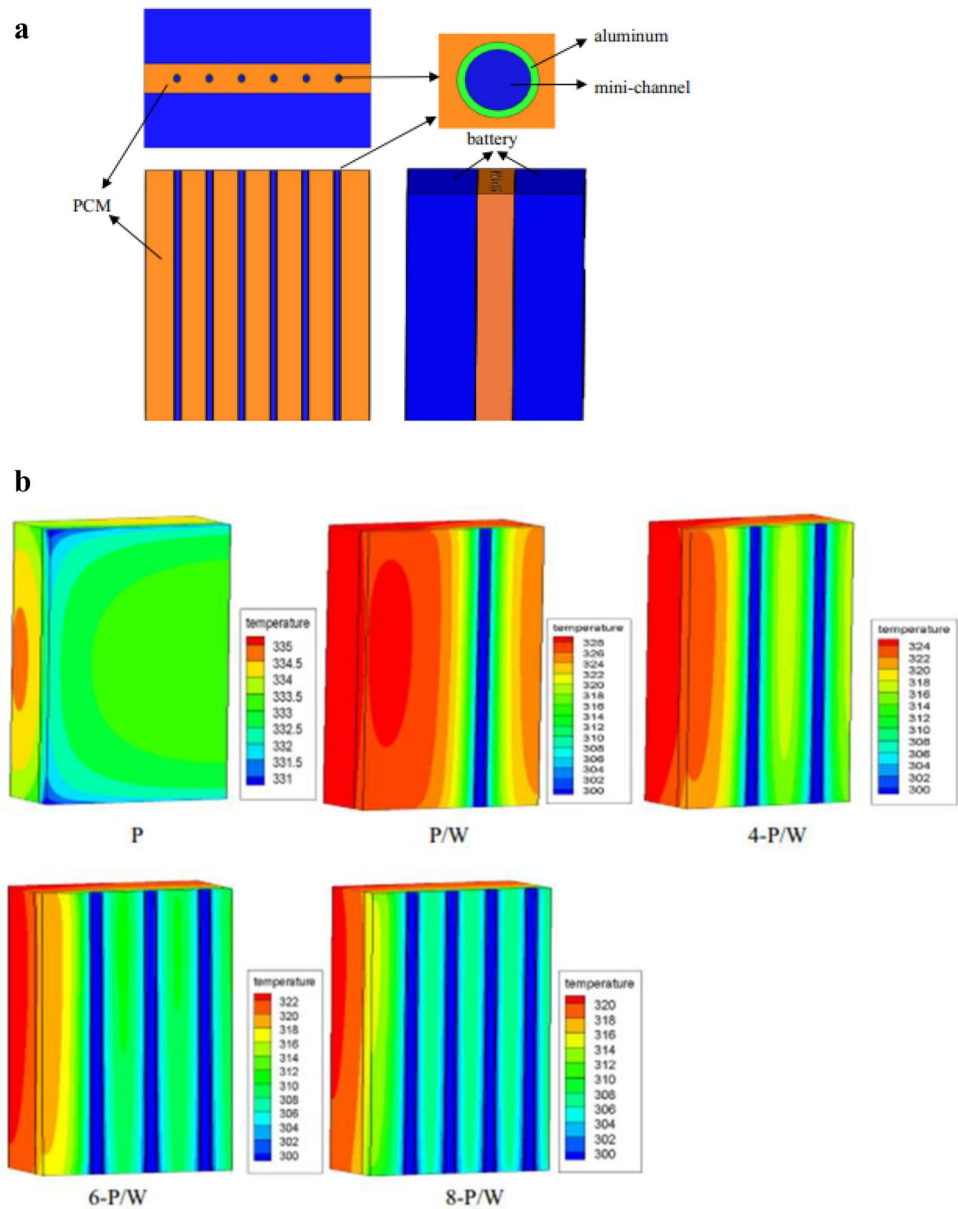


Fig. 65 Comparison of dry and spray cooling [125]

In order to evaluate the effectiveness of mist cooling, a 6-celled circularly arranged battery module was created using SolidWorks software by Saw et al. [126]. To enhance the heat transfer and prevent issues like short circuits and corrosion, Boron Nitride coating was applied to both the bodies and terminals of the batteries. The flow conditions were analysed using the k - ϵ turbulence model and a dispersed fluid model for mist flow in ANSYS CFX. The results showed that introducing an amount of mist into air significantly improved heat transfer performance. The research suggests that maintaining a surface temperature below 40 °C and a temperature difference below 5 °C during charging at 3C rate can be achieved with an inlet mass flow rate of 5 g/s and a 3% mist loading fraction as in Fig. 66. Mist cooling demonstrated a 45% improvement

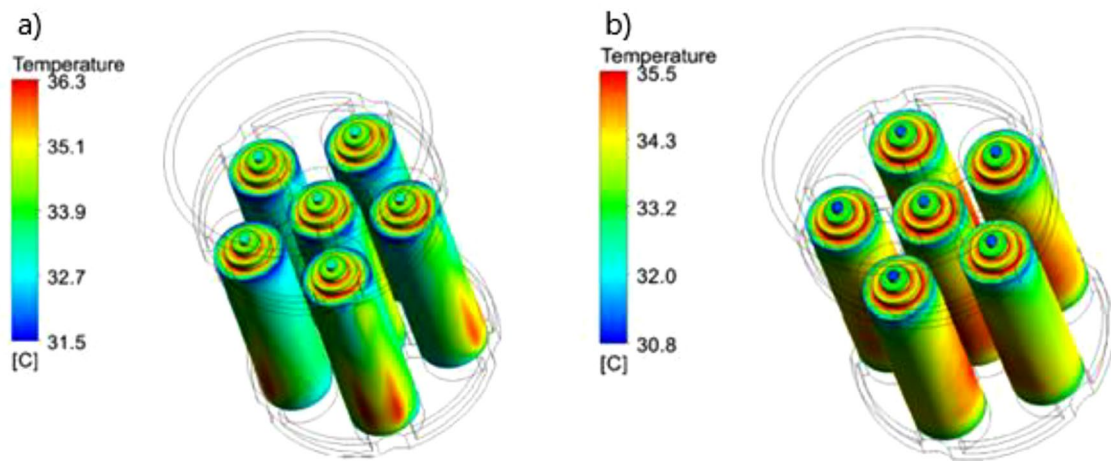


Fig. 66 Temperature contour for **a** conventional air cooling and **b** mist cooling [126]

in performance compared to forced convection while consuming power.

Numerical analysis by Kumari et al. [127] investigate the improvement endorsed on introducing mist flow instead of air flow in heat sinks and revealed a 97% reduction in resistance with mist cooling compared with active air cooling. The influence of the droplet size and the quantity of mist loaded on the evaporation of the mist drops was stated as the droplet evaporation impacts the thermal performance.

6 Discussion

By analysing various types of BTMS by numerical simulations showed that the cheap air cooled BTMS with simple structure suits almost all battery models but has reduced thermal performance and providing forced cooling can account for further improvement. The improvement on changing the flow channel designs, battery arrangement, fan placement was evident. The liquid cooled BTMS operates with high efficiency providing homogeneous distribution of temperature with the expense of parasitic power consumption of the instruments included increasing the complexity of the system. The modification of channel design, number of channels, distribution of coolant in the channel, coolant mass flow rates affect the system performance. The coolant mass flow rate for specific inlet temperature has to be optimised proving a trade-off with pressure drop in the channels of coolant flow. In liquid cooling, the area of nanofluids can still be explored due to the excellent thermal properties of nanofluids compared with conventional can account for improved thermal performance considering the effects of sedimentation, agglomeration and pressure drop. Immersion cooling/Direct cooling with the aid of high specific

heat capacity dielectric fluids is effective as the hot surfaces of the battery is in direct fluid contact and with the risk in the leakage of coolants and its performance can be further enhanced by the application of phase change fluids having high latent heat. Among the passive cooling, PCM provides temperature homogeneity but the cooling efficiency is low. Heat pipes suitable for both heating and cooling applications can account for thermal control but during thermal abuse conditions it faces a drawback. A boosted performance is attained when these passive systems are combined with the other cooling systems mostly with liquid cooling system and improvement in PCM can also account for further performance. Additionally, further augmentation of thermal management systems can be done with the aid of evaporative cooling, mist/spray cooling techniques.

Among the various CFD packages used in running numerical simulations, ANSYS FLUENT was discovered to be the most popular platform utilized during the modelling of thermal performance of BTMS by authors; in certain situations, COMSOL Multiphysics is also used. The k - ϵ turbulence model is mostly used to simulate the flow and heat transfer characteristics. For the case of passive cooling, the multiphase models and volume of fluid models are also adapted. The heat source model is critical for accurate prediction of outcomes, and frequently generalized heat source model is employed and for high accuracy results the MSMD models having non-uniform heat generation is employed as it provides a more comprehensive and detailed understanding of large-format battery cells, which are often used in applications like electric vehicles and is crucial for optimizing battery performance, ensuring safety, and extending battery lifespan but increases the computational complexity when compared to simple lumped-parameter models of uniform heat generation. Additionally, it has been noticed that the optimization of BTMS for better thermal performance are

multi-objective problems with a variety of functional constraints. The experimental validation and the findings of the numerical analyses are in strong agreement, demonstrating the validity of the CFD models for the examination of various BTMS kinds.

In spite of having many solutions to the BTMS of EV, the commercial viability of the solution is not ensured. Thereby, the future researchers can utilize the high performing CFD model to trace out the best system of thermal management considering the extreme conditions of ambient and fast charging. Further, the best model can be fabricated and benchmarking that system for specified operating conditions can lead to the development of commercially acceptable solutions.

7 Conclusion

The primary energy storage system for electric vehicles (EVs), Li-ion batteries are prone to both operational and ambient temperatures. Any mismanagement of a battery pack's vital temperature pattern, including the temperature range and uniformity, may negatively affect the battery's lifespan, capacity deterioration, and, in certain severe circumstances, a safety threat like thermal runaway and explosion. Because it maintains the battery within an ideal temperature range, the Battery Thermal Management System (BTMS) is crucial to the whole EV's safety and performance. The primary goal of this review is on the numerical and CFD analysis of different BTMS, including air, liquid, PCM, and hybrids cooling strategies, as the thermal performance of the BTMS observed in the CFD analysis can boost the confidence of the researcher for its practical viability as the researcher acquires understanding of the flow field and temperature response, which is challenging to observe in the experiment. Using different CFD tools having various turbulent models like $k-\epsilon$, $k-\omega$, RANS, the researchers reported that the projected outcomes and the outcomes of the experiment are well-aligned and Dispersed fluid model, Volume of fluid model were employed based on the methods of BTMS employed. The results predicted using the Multi Scale Multi Domain (MSMD) heat source model accompanied with the Equivalent Circuit Model (ECM) provides more reliable solution as it accounts almost all the possible heat generation in the battery. Some researchers incorporated multi objective optimisation techniques for maximized thermal performance with minimized pressure drop by the controlling the design and operational parameters of the BTMS. It can be concluded that that CFD analysis could be employed across diverse operation conditions of various strategies of thermal management of batteries confidently by the researchers and further optimisation can pave the way for

experimentation and commercialisation of the high performing thermal management system.

8 Future Scope

A wide scope for future research is envisaged from the exclusive review made on the numerical analysis of various thermal management strategies and the notable gaps which remain intact in the research field are,

- Even though performance of active cooling strategies is significant under extreme conditions, considerable parasitic power consumption in active system opens a wide scope in developing efficient passive (or) hybrid systems.
- In passive systems, the loop heat pipes (LHP) can be investigated in superior compared to PCM having lesser life cycle time than LHP.
- The impact of varying loads on the electric vehicle that affects the motor temperature causing power loss in the traction system and the effect of the state-of-charge of the battery on the parasitic power consumption of the active cooling systems is to be explored.
- The thermal performance of the strategy employed in the battery is evaluated based on the effects of conduction and convection only. This evidently marks the scope of considering the radiation effects in the analysis of thermal management strategy.
- The influence of vibrations on the strategies involving volume of fluid (VOF) model such as immersion cooling, PCM has to be investigated.
- The numerical studies mainly prioritize the thermal design of the strategy neglecting the structural design of the cooling system. The effects of additional weights on modified cooling strategy, the space requirements to fit in system and structural integrity of the systems has to be considered.

References

1. Akinlabi AAH, Solyali D (2020) Configuration, design, and optimization of air-cooled battery thermal management system for electric vehicles: a review. *Renew Sustain Energy Rev* 125:109815. <https://doi.org/10.1016/j.rser.2020.109815>
2. Mazumder H, Hassan MMAE, Ektesabi M, Kapoor A (2012) Performance analysis of EV for different mass distributions to ensure safe handling. *Energy Procedia* 14:949–954. <https://doi.org/10.1016/j.egypro.2011.12.1038>
3. Pelegov D, Pontes J (2018) Main drivers of battery industry changes: electric vehicles—a market overview. *Batteries* 4:65. <https://doi.org/10.3390/batteries4040065>

4. Olivetti EA, Ceder G, Gaustad GG, Fu X (2017) Lithium-ion battery supply chain considerations: analysis of potential bottlenecks in critical metals. *Joule* 1:229–243. <https://doi.org/10.1016/j.joule.2017.08.019>
5. Reddy T (2010) *Linden's handbook of batteries*, 4th edn. McGraw Hill Professional, New York
6. Hu M, Pang X, Zhou Z (2013) Recent progress in high-voltage lithium ion batteries. *J Power Sources* 237:229–242. <https://doi.org/10.1016/j.jpowsour.2013.03.024>
7. Xia Q, Yang D, Wang Z et al (2020) Multiphysical modeling for life analysis of lithium-ion battery pack in electric vehicles. *Renew Sustain Energy Rev* 131:109993. <https://doi.org/10.1016/j.rser.2020.109993>
8. Shim J (2002) Electrochemical analysis for cycle performance and capacity fading of a lithium-ion battery cycled at elevated temperature. *J Power Sources* 112:222–230. [https://doi.org/10.1016/s0378-7753\(02\)00363-4](https://doi.org/10.1016/s0378-7753(02)00363-4)
9. Wang Q, Ping P, Zhao X et al (2012) Thermal runaway caused fire and explosion of lithium ion battery. *J Power Sources* 208:210–224. <https://doi.org/10.1016/j.jpowsour.2012.02.038>
10. Zhang SS, Xu K, Jow TR (2003) The low temperature performance of Li-ion batteries. *J Power Sources* 115:137–140. [https://doi.org/10.1016/s0378-7753\(02\)00618-3](https://doi.org/10.1016/s0378-7753(02)00618-3)
11. Jaguemont J, Boulon L, Dubé Y (2016) A comprehensive review of lithium-ion batteries used in hybrid and electric vehicles at cold temperatures. *Appl Energy* 164:99–114. <https://doi.org/10.1016/j.apenergy.2015.11.034>
12. Pesaran A, Santhanagopalan S, Kim GH (2013) Addressing the impact of temperature extremes on large format Li-ion batteries for vehicle applications (presentation) (No. NREL/PR-5400-58145). National Renewable Energy Laboratory (NREL), Golden
13. Mi C, Li B, Buck D, Ota N (2007) Advanced electro-thermal modeling of lithium-ion battery system for hybrid electric vehicle applications. In: 2007 IEEE vehicle power and propulsion conference, 2007. IEEE, pp 107–111
14. Bandhauer TM, Garimella S, Fuller TF (2011) A critical review of thermal issues in lithium-ion batteries. *J Electrochem Soc* 158:R1. <https://doi.org/10.1149/1.3515880>
15. Pesaran AA (2001) Battery thermal management in EV and HEVs: issues and solutions. *Battery Man* 43(5):34–49
16. Xia G, Cao L, Bi G (2017) A review on battery thermal management in electric vehicle application. *J Power Sources* 367:90–105. <https://doi.org/10.1016/j.jpowsour.2017.09.046>
17. Pesaran AA (2002) Battery thermal models for hybrid vehicle simulations. *J Power Sources* 110:377–382. [https://doi.org/10.1016/s0378-7753\(02\)00200-8](https://doi.org/10.1016/s0378-7753(02)00200-8)
18. Kumar Thakur A, Sathyamurthy R, Velraj R et al (2023) A state-of-the-art review on advancing battery thermal management systems for fast-charging. *Appl Therm Eng* 226:120303. <https://doi.org/10.1016/j.applthermaleng.2023.120303>
19. Ning G, Haran B, Popov BN (2003) Capacity fade study of lithium-ion batteries cycled at high discharge rates. *J Power Sources* 117:160–169. [https://doi.org/10.1016/s0378-7753\(03\)00029-6](https://doi.org/10.1016/s0378-7753(03)00029-6)
20. Cicconi P, Landi D, Germani M (2017) Thermal analysis and simulation of a Li-ion battery pack for a lightweight commercial EV. *Appl Energy* 192:159–177. <https://doi.org/10.1016/j.apenergy.2017.02.008>
21. Williford RE, Viswanathan VV, Zhang J-G (2009) Effects of entropy changes in anodes and cathodes on the thermal behavior of lithium ion batteries. *J Power Sources* 189:101–107. <https://doi.org/10.1016/j.jpowsour.2008.10.078>
22. Lin C, Chen K, Sun F, Tang P, Zhao H (2009) Research on thermo-physical properties identification and thermal analysis of EV Li-ion battery. In: 2009 IEEE vehicle power and propulsion conference, 2009. IEEE, pp 1643–1648
23. Arora S (2018) Selection of thermal management system for modular battery packs of electric vehicles: a review of existing and emerging technologies. *J Power Sources* 400:621–640. <https://doi.org/10.1016/j.jpowsour.2018.08.020>
24. Sabbah R, Kizilel R, Selman JR, Al-Hallaj S (2008) Active (air-cooled) vs. passive (phase change material) thermal management of high power lithium-ion packs: limitation of temperature rise and uniformity of temperature distribution. *J Power Sources* 182:630–638. <https://doi.org/10.1016/j.jpowsour.2008.03.082>
25. Offer G, Patel Y, Hales A et al (2020) Cool metric for lithium-ion batteries could spur progress. *Nature* 582:485–487. <https://doi.org/10.1038/d41586-020-01813-8>
26. Pesaran A, Keyser M, Burch S (1999) An approach for designing thermal management systems for electric and hybrid vehicle battery packs (No. NREL/CP-540-25992). National Renewable Energy Laboratory, Golden
27. Liu H, Wei Z, He W, Zhao J (2017) Thermal issues about Li-ion batteries and recent progress in battery thermal management systems: a review. *Energy Convers Manag* 150:304–330. <https://doi.org/10.1016/j.enconman.2017.08.016>
28. Rao Z, Wang S (2011) A review of power battery thermal energy management. *Renew Sustain Energy Rev* 15:4554–4571. <https://doi.org/10.1016/j.rser.2011.07.096>
29. Al-Zareer M, Dincer I, Rosen MA (2018) A review of novel thermal management systems for batteries. *Int J Energy Res* 42:3182–3205. <https://doi.org/10.1002/er.4095>
30. Lu M, Zhang X, Ji J et al (2020) Research progress on power battery cooling technology for electric vehicles. *J Energy Storage* 27:101155. <https://doi.org/10.1016/j.est.2019.101155>
31. Zhao C, Cao W, Dong T, Jiang F (2018) Thermal behavior study of discharging/charging cylindrical lithium-ion battery module cooled by channeled liquid flow. *Int J Heat Mass Transf* 120:751–762. <https://doi.org/10.1016/j.ijheatmasstransfer.2017.12.083>
32. Roe C, Feng X, White G et al (2022) Immersion cooling for lithium-ion batteries—a review. *J Power Sources* 525:231094. <https://doi.org/10.1016/j.jpowsour.2022.231094>
33. Faghri A, Harley C (1994) Transient lumped heat pipe analyses. *Heat Recovery Syst CHP* 14:351–363. [https://doi.org/10.1016/0890-4332\(94\)90039-6](https://doi.org/10.1016/0890-4332(94)90039-6)
34. Abramushkina E, Zhaksylyk A, Geury T et al (2021) A thorough review of cooling concepts and thermal management techniques for automotive WBG inverters: topology, technology and integration level. *Energies* 14:4981. <https://doi.org/10.3390/en14164981>
35. El Idi MM, Karkri M, Abdou Tankari M (2021) A passive thermal management system of Li-ion batteries using PCM composites: experimental and numerical investigations. *Int J Heat Mass Transf* 169:120894. <https://doi.org/10.1016/j.ijheatmasstransfer.2020.120894>
36. Xiao Y, Bai D, Xie Z et al (2021) Flexible copper foam-based phase change materials with good stiffness-toughness balance, electro-to-thermal conversion ability and shape memory function for intelligent thermal management. *Composites A* 146:106420. <https://doi.org/10.1016/j.compositesa.2021.106420>
37. Wang D, Niu X, Yan Y et al (2021) Research on falling film dehumidification performance of microencapsulated phase change materials slurry. *Energy Build* 235:110750. <https://doi.org/10.1016/j.enbuild.2021.110750>
38. Ismail NHF, Toha SF, Azubir NAM et al (2013) Simplified heat generation model for lithium ion battery used in electric vehicle. *IOP Conf Ser Mater Sci Eng* 53:012014. <https://doi.org/10.1088/1757-899x/53/1/012014>
39. Immonen E, Hurri J (2021) Incremental thermo-electric CFD modeling of a high-energy Lithium-Titanate Oxide battery cell in different temperatures: a comparative study. *Appl Therm Eng* 197:117260. <https://doi.org/10.1016/j.applthermaleng.2021.117260>

40. Huria T, Ceraolo M, Gazzarri J, Jackey R (2012) High fidelity electrical model with thermal dependence for characterization and simulation of high power lithium battery cells. In: 2012 IEEE international electric vehicle conference, 2012. IEEE, pp 1–8
41. Bernardi D, Pawlikowski E, Newman J (1985) A general energy balance for battery systems. *J Electrochem Soc* 132:5–12. <https://doi.org/10.1149/1.2113792>
42. Kim US, Shin CB, Kim C-S (2008) Effect of electrode configuration on the thermal behavior of a lithium-polymer battery. *J Power Sources* 180:909–916. <https://doi.org/10.1016/j.jpowsour.2007.09.054>
43. Kim G-H, Smith K, Lee K-J et al (2011) Multi-domain modeling of lithium-ion batteries encompassing multi-physics in varied length scales. *J Electrochem Soc* 158:A955. <https://doi.org/10.1149/1.3597614>
44. Kim US, Shin CB, Kim C-S (2009) Modeling for the scale-up of a lithium-ion polymer battery. *J Power Sources* 189:841–846. <https://doi.org/10.1016/j.jpowsour.2008.10.019>
45. Rao R, Vrudhula S, Rakhmatov DN (2003) Battery modeling for energy-aware system design. *Computer* 36:77–87. <https://doi.org/10.1109/mc.2003.1250886>
46. Chen M, Rincon-Mora GA (2006) Accurate electrical battery model capable of predicting runtime and IV performance. *IEEE Trans Energy Convers* 21(2):504–511
47. Kummitha OR (2023) Thermal cooling of Li-ion cylindrical cells battery module with baffles arrangement for airflow cooling numerical analysis. *J Energy Storage* 59:106474. <https://doi.org/10.1016/j.est.2022.106474>
48. Karatas OB, Sokmen KF (2022) Thermal optimization of inter-cellular distance in lithium-ion batteries and numerical analysis of the original honeycomb metal integrated battery pack. *J Energy Storage* 55:105705. <https://doi.org/10.1016/j.est.2022.105705>
49. Alharbi KAM, Smaism GF, Sajadi SM et al (2022) Numerical study of lozenge, triangular and rectangular arrangements of lithium-ion batteries in their thermal management in a cooled-air cooling system. *J Energy Storage* 52:104786. <https://doi.org/10.1016/j.est.2022.104786>
50. Öztöp M, Şahinaslan A (2022) Control of temperature distribution for Li-ion battery modules via longitudinal fins. *J Energy Storage* 52:104760. <https://doi.org/10.1016/j.est.2022.104760>
51. Saechan P, Dhuchakallaya I (2022) Numerical study on the air-cooled thermal management of lithium-ion battery pack for electrical vehicles. *Energy Rep* 8:1264–1270. <https://doi.org/10.1016/j.egyr.2021.11.089>
52. Jiaqiang E, Yue M, Chen J et al (2018) Effects of the different air cooling strategies on cooling performance of a lithium-ion battery module with baffle. *Appl Therm Eng* 144:231–241. <https://doi.org/10.1016/j.applthermaleng.2018.08.064>
53. Saw LH, Ye Y, Tay AAO et al (2016) Computational fluid dynamic and thermal analysis of lithium-ion battery pack with air cooling. *Appl Energy* 177:783–792. <https://doi.org/10.1016/j.apenergy.2016.05.122>
54. Yu K, Yang X, Cheng Y, Li C (2014) Thermal analysis and two-directional air flow thermal management for lithium-ion battery pack. *J Power Sources* 270:193–200. <https://doi.org/10.1016/j.jpowsour.2014.07.086>
55. Wang T, Tseng KJ, Zhao J, Wei Z (2014) Thermal investigation of lithium-ion battery module with different cell arrangement structures and forced air-cooling strategies. *Appl Energy* 134:229–238. <https://doi.org/10.1016/j.apenergy.2014.08.013>
56. Fan L, Khodadadi JM, Pesaran AA (2013) A parametric study on thermal management of an air-cooled lithium-ion battery module for plug-in hybrid electric vehicles. *J Power Sources* 238:301–312. <https://doi.org/10.1016/j.jpowsour.2013.03.050>
57. Saw LH, Ye Y, Yew MC et al (2017) Computational fluid dynamics simulation on open cell aluminium foams for Li-ion battery cooling system. *Appl Energy* 204:1489–1499. <https://doi.org/10.1016/j.apenergy.2017.04.022>
58. Mohammadian SK, Rassoulinejad-Mousavi SM, Zhang Y (2015) Thermal management improvement of an air-cooled high-power lithium-ion battery by embedding metal foam. *J Power Sources* 296:305–313. <https://doi.org/10.1016/j.jpowsour.2015.07.056>
59. Sarvar-Ardeh S, Rafee R, Rashidi S (2023) Enhancing the performance of liquid-based battery thermal management system by porous substrate minichannel. *J Energy Storage* 71:108142. <https://doi.org/10.1016/j.est.2023.108142>
60. Adeniran A, Park S (2023) Optimized cooling and thermal analysis of lithium-ion pouch cell under fast charging cycles for electric vehicles. *J Energy Storage* 68:107580. <https://doi.org/10.1016/j.est.2023.107580>
61. Verma A, Saikia T, Saikia P et al (2023) Thermal performance analysis and experimental verification of lithium-ion batteries for electric vehicle applications through optimized inclined mini-channels. *Appl Energy* 335:120743. <https://doi.org/10.1016/j.apenergy.2023.120743>
62. Lai C, Shan S, Feng S et al (2023) Numerical investigations on heat transfer enhancement and energy flow distribution for interlayer battery thermal management system using Tesla-valve mini-channel cooling. *Energy Convers Manag* 280:116812. <https://doi.org/10.1016/j.enconman.2023.116812>
63. Han J, Ko W, Lim M-S et al (2023) A numerical study of enhanced lithium-ion battery cooling using a module insert. *Case Stud Therm Eng* 42:102751. <https://doi.org/10.1016/j.csite.2023.102751>
64. Guo R, Li L (2022) Heat dissipation analysis and optimization of lithium-ion batteries with a novel parallel-spiral serpentine channel liquid cooling plate. *Int J Heat Mass Transf* 189:122706. <https://doi.org/10.1016/j.ijheatmasstransfer.2022.122706>
65. Zuo W, Zhang Y, Jiaqiang E et al (2022) Performance comparison between single S-channel and double S-channel cold plate for thermal management of a prismatic LiFePO₄ battery. *Renew Energy* 192:46–57. <https://doi.org/10.1016/j.renene.2022.04.116>
66. Tang Z, Liu Z, Li J, Cheng J (2021) A lightweight liquid cooling thermal management structure for prismatic batteries. *J Energy Storage* 42:103078. <https://doi.org/10.1016/j.est.2021.103078>
67. Deng T, Zhang G, Ran Y, Liu P (2019) Thermal performance of lithium ion battery pack by using cold plate. *Appl Therm Eng* 160:114088. <https://doi.org/10.1016/j.applthermaleng.2019.114088>
68. Liu H, Shi H, Shen H, Xie G (2019) The performance management of a Li-ion battery by using tree-like mini-channel heat sinks: experimental and numerical optimization. *Energy* 189:116150. <https://doi.org/10.1016/j.energy.2019.116150>
69. Zhao C, Sousa ACM, Jiang F (2019) Minimization of thermal non-uniformity in lithium-ion battery pack cooled by channeled liquid flow. *Int J Heat Mass Transf* 129:660–670. <https://doi.org/10.1016/j.ijheatmasstransfer.2018.10.017>
70. Xu X, Li W, Xu B, Qin J (2019) Numerical study on a water cooling system for prismatic LiFePO₄ batteries at abused operating conditions. *Appl Energy* 250:404–412. <https://doi.org/10.1016/j.apenergy.2019.04.180>
71. Zhou H, Zhou F, Zhang Q et al (2019) Thermal management of cylindrical lithium-ion battery based on a liquid cooling method with half-helical duct. *Appl Therm Eng* 162:114257. <https://doi.org/10.1016/j.applthermaleng.2019.114257>
72. Li X, He F, Zhang G et al (2019) Experiment and simulation for pouch battery with silica cooling plates and copper mesh based air cooling thermal management system. *Appl Therm Eng*

- 146:866–880. <https://doi.org/10.1016/j.applthermaleng.2018.10.061>
73. Panchal S, Khasow R, Dincer I et al (2017) Thermal design and simulation of mini-channel cold plate for water cooled large sized prismatic lithium-ion battery. *Appl Therm Eng* 122:80–90. <https://doi.org/10.1016/j.applthermaleng.2017.05.010>
 74. De Vita A, Maheshwari A, Destro M et al (2017) Transient thermal analysis of a lithium-ion battery pack comparing different cooling solutions for automotive applications. *Appl Energy* 206:101–112. <https://doi.org/10.1016/j.apenergy.2017.08.184>
 75. Qian Z, Li Y, Rao Z (2016) Thermal performance of lithium-ion battery thermal management system by using mini-channel cooling. *Energy Convers Manag* 126:622–631. <https://doi.org/10.1016/j.enconman.2016.08.063>
 76. Zhao J, Rao Z, Li Y (2015) Thermal performance of mini-channel liquid cooled cylinder based battery thermal management for cylindrical lithium-ion power battery. *Energy Convers Manag* 103:157–165. <https://doi.org/10.1016/j.enconman.2015.06.056>
 77. Huo Y, Rao Z, Liu X, Zhao J (2015) Investigation of power battery thermal management by using mini-channel cold plate. *Energy Convers Manag* 89:387–395. <https://doi.org/10.1016/j.enconman.2014.10.015>
 78. Liu J, Ma Q, Li X (2023) Numerical study on heat dissipation performance of a lithium-ion battery module based on immersion cooling. *J Energy Storage* 66:107511. <https://doi.org/10.1016/j.est.2023.107511>
 79. Jindal P, Sharma P, Kundu M et al (2022) Computational Fluid Dynamics (CFD) analysis of Graphene Nanoplatelets for the cooling of a multiple tier Li-ion battery pack. *Therm Sci Eng Prog* 31:101282. <https://doi.org/10.1016/j.tsep.2022.101282>
 80. Cao Y, Mansir IB, Mouldi A et al (2022) Designing a system for battery thermal management: cooling LIBs by nano-encapsulated phase change material. *Case Stud Therm Eng* 33:101943. <https://doi.org/10.1016/j.csite.2022.101943>
 81. Jithin KV, Rajesh PK (2022) Numerical analysis of single-phase liquid immersion cooling for lithium-ion battery thermal management using different dielectric fluids. *Int J Heat Mass Transf* 188:122608. <https://doi.org/10.1016/j.ijheatmasstransfer.2022.122608>
 82. Tan X, Lyu P, Fan Y et al (2021) Numerical investigation of the direct liquid cooling of a fast-charging lithium-ion battery pack in hydrofluoroether. *Appl Therm Eng* 196:117279. <https://doi.org/10.1016/j.applthermaleng.2021.117279>
 83. Huo Y, Rao Z (2015) The numerical investigation of nanofluid based cylinder battery thermal management using lattice Boltzmann method. *Int J Heat Mass Transf* 91:374–384. <https://doi.org/10.1016/j.ijheatmasstransfer.2015.07.128>
 84. Alihosseini A, Shafaei M (2021) Experimental study and numerical simulation of a Lithium-ion battery thermal management system using a heat pipe. *J Energy Storage* 39:102616. <https://doi.org/10.1016/j.est.2021.102616>
 85. Bernagozzi M, Georgoulas A, Miché N et al (2021) Novel battery thermal management system for electric vehicles with a loop heat pipe and graphite sheet inserts. *Appl Therm Eng* 194:117061. <https://doi.org/10.1016/j.applthermaleng.2021.117061>
 86. Wang L, Zhao Y, Quan Z, Liang J (2021) Investigation of thermal management of lithium-ion battery based on micro heat pipe array. *J Energy Storage* 39:102624. <https://doi.org/10.1016/j.est.2021.102624>
 87. Kleiner J, Singh R, Schmid M et al (2021) Influence of heat pipe assisted terminal cooling on the thermal behavior of a large prismatic lithium-ion cell during fast charging in electric vehicles. *Appl Therm Eng* 188:116328. <https://doi.org/10.1016/j.applthermaleng.2020.116328>
 88. Liang Z, Wang R, Malt AH et al (2021) Systematic evaluation of a flat-heat-pipe-based thermal management: cell-to-cell variations and battery ageing. *Appl Therm Eng* 192:116934. <https://doi.org/10.1016/j.applthermaleng.2021.116934>
 89. Greco A, Cao D, Jiang X, Yang H (2014) A theoretical and computational study of lithium-ion battery thermal management for electric vehicles using heat pipes. *J Power Sources* 257:344–355. <https://doi.org/10.1016/j.jpowsour.2014.02.004>
 90. Li Y, Qi F, Guo H et al (2019) Numerical investigation of thermal runaway propagation in a Li-ion battery module using the heat pipe cooling system. *Numer Heat Transf A* 75:183–199. <https://doi.org/10.1080/10407782.2019.1580956>
 91. Yang M, Nicholls RA, Moghimi MA, Griffiths AL (2023) Performance management of EV battery coupled with latent heat jacket at cell level. *J Power Sources* 558:232618. <https://doi.org/10.1016/j.jpowsour.2022.232618>
 92. Li Y, Chen Z, Feng Y et al (2023) A novel petal-type battery thermal management system with dual phase change materials. *Int J Heat Mass Transf* 207:123989. <https://doi.org/10.1016/j.ijheatmasstransfer.2023.123989>
 93. Zhang F, Lu F, Liang B et al (2023) Thermal performance analysis of a new type of branch-fin enhanced battery thermal management PCM module. *Renew Energy* 206:1049–1063. <https://doi.org/10.1016/j.renene.2023.02.083>
 94. Verma A, Rakshit D (2022) Performance analysis of PCM-fin combination for heat abatement of Li-ion battery pack in electric vehicles at high ambient temperature. *Therm Sci Eng Prog* 32:101314. <https://doi.org/10.1016/j.tsep.2022.101314>
 95. Jilte R, Afzal A, Panchal S (2021) A novel battery thermal management system using nano-enhanced phase change materials. *Energy* 219:119564. <https://doi.org/10.1016/j.energy.2020.119564>
 96. Sun Z, Fan R, Yan F et al (2019) Thermal management of the lithium-ion battery by the composite PCM-Fin structures. *Int J Heat Mass Transf* 145:118739. <https://doi.org/10.1016/j.ijheatmasstransfer.2019.118739>
 97. Ranjbaran YS, Haghparast SJ, Shojaeefard MH, Molaeimanesh GR (2019) Numerical evaluation of a thermal management system consisting PCM and porous metal foam for Li-ion batteries. *J Therm Anal Calorim* 141:1717–1739. <https://doi.org/10.1007/s10973-019-08989-w>
 98. Verma A, Shashidhara S, Rakshit D (2019) A comparative study on battery thermal management using phase change material (PCM). *Therm Sci Eng Prog* 11:74–83. <https://doi.org/10.1016/j.tsep.2019.03.003>
 99. Al-Zareer M, Dincer I, Rosen MA (2018) A novel phase change based cooling system for prismatic lithium ion batteries. *Int J Refrig* 86:203–217. <https://doi.org/10.1016/j.ijrefrig.2017.12.005>
 100. Greco A, Jiang X, Cao D (2015) An investigation of lithium-ion battery thermal management using paraffin/porous-graphite-matrix composite. *J Power Sources* 278:50–68. <https://doi.org/10.1016/j.jpowsour.2014.12.027>
 101. Javani N, Dincer I, Naterer GF, Yilbas BS (2014) Heat transfer and thermal management with PCMs in a Li-ion battery cell for electric vehicles. *Int J Heat Mass Transf* 72:690–703. <https://doi.org/10.1016/j.ijheatmasstransfer.2013.12.076>
 102. Choi H, Lee H, Kim J, Lee H (2023) Hybrid single-phase immersion cooling structure for battery thermal management under fast-charging conditions. *Energy Convers Manag* 287:117053. <https://doi.org/10.1016/j.enconman.2023.117053>
 103. Chen S, Wang R, Bao H et al (2023) Numerical investigation of form-stable composite phase change material for battery passive cooling. *Case Stud Therm Eng* 50:103410. <https://doi.org/10.1016/j.csite.2023.103410>
 104. Mousavi S, Zadehkabir A, Siavashi M, Yang X (2023) An improved hybrid thermal management system for prismatic Li-ion batteries integrated with mini-channel and phase change

- materials. *Appl Energy* 334:120643. <https://doi.org/10.1016/j.apenergy.2023.120643>
105. Rabiei M, Gharehghani A, Andwari AM (2023) Enhancement of battery thermal management system using a novel structure of hybrid liquid cold plate. *Appl Therm Eng* 232:121051. <https://doi.org/10.1016/j.applthermaleng.2023.121051>
 106. Angani A, Kim H-W, Hwang M-H et al (2023) A comparison between Zig-Zag plated hybrid parallel pipe and liquid cooling battery thermal management systems for Lithium-ion battery module. *Appl Therm Eng* 219:119599. <https://doi.org/10.1016/j.applthermaleng.2022.119599>
 107. Chen X, Zhou F, Yang W et al (2022) A hybrid thermal management system with liquid cooling and composite phase change materials containing various expanded graphite contents for cylindrical lithium-ion batteries. *Appl Therm Eng* 200:117702. <https://doi.org/10.1016/j.applthermaleng.2021.117702>
 108. Zeng W, Niu Y, Li S et al (2022) Cooling performance and optimization of a new hybrid thermal management system of cylindrical battery. *Appl Therm Eng* 217:119171. <https://doi.org/10.1016/j.applthermaleng.2022.119171>
 109. Hekmat S, Bamdezh MA, Molaieimaneh GR (2022) Hybrid thermal management for achieving extremely uniform temperature distribution in a lithium battery module with phase change material and liquid cooling channels. *J Energy Storage* 50:104272. <https://doi.org/10.1016/j.est.2022.104272>
 110. Shahid S, Chea B, Agelin-Chaab M (2022) Development of a hybrid cooling concept for cylindrical Li-ion cells. *J Energy Storage* 50:104214. <https://doi.org/10.1016/j.est.2022.104214>
 111. Akbarzadeh M, Jaguemont J, Kalogiannis T et al (2021) A novel liquid cooling plate concept for thermal management of lithium-ion batteries in electric vehicles. *Energy Convers Manag* 231:113862. <https://doi.org/10.1016/j.enconman.2021.113862>
 112. Li Y, Guo H, Qi F et al (2021) Investigation on liquid cold plate thermal management system with heat pipes for LiFePO₄ battery pack in electric vehicles. *Appl Therm Eng* 185:116382. <https://doi.org/10.1016/j.applthermaleng.2020.116382>
 113. Karimi D, Hosen MS, Behi H et al (2021) A hybrid thermal management system for high power lithium-ion capacitors combining heat pipe with phase change materials. *Heliyon* 7:e07773. <https://doi.org/10.1016/j.heliyon.2021.e07773>
 114. Safdari M, Ahmadi R, Sadeghzadeh S (2020) Numerical investigation on PCM encapsulation shape used in the passive-active battery thermal management. *Energy* 193:116840. <https://doi.org/10.1016/j.energy.2019.116840>
 115. Behi H, Karimi D, Behi M et al (2020) A new concept of thermal management system in Li-ion battery using air cooling and heat pipe for electric vehicles. *Appl Therm Eng* 174:115280. <https://doi.org/10.1016/j.applthermaleng.2020.115280>
 116. Gan Y, He L, Liang J et al (2020) A numerical study on the performance of a thermal management system for a battery pack with cylindrical cells based on heat pipes. *Appl Therm Eng* 179:115740. <https://doi.org/10.1016/j.applthermaleng.2020.115740>
 117. Zhang Z, Wei K (2020) Experimental and numerical study of a passive thermal management system using flat heat pipes for lithium-ion batteries. *Appl Therm Eng* 166:114660. <https://doi.org/10.1016/j.applthermaleng.2019.114660>
 118. Xie Y, Tang J, Shi S et al (2017) Experimental and numerical investigation on integrated thermal management for lithium-ion battery pack with composite phase change materials. *Energy Convers Manag* 154:562–575. <https://doi.org/10.1016/j.enconman.2017.11.046>
 119. Rao Z, Wang Q, Huang C (2016) Investigation of the thermal performance of phase change material/mini-channel coupled battery thermal management system. *Appl Energy* 164:659–669. <https://doi.org/10.1016/j.apenergy.2015.12.021>
 120. Zhao Y, Patel Y, Zhang T, Offer GJ (2018) Modeling the effects of thermal gradients induced by tab and surface cooling on lithium ion cell performance. *J Electrochem Soc* 165:A3169–A3178. <https://doi.org/10.1149/2.0901813jes>
 121. Hunt IA, Zhao Y, Patel Y, Offer J (2016) Surface cooling causes accelerated degradation compared to tab cooling for lithium-ion pouch cells. *J Electrochem Soc* 163:A1846–A1852. <https://doi.org/10.1149/2.0361609jes>
 122. Dondelewski O, Szemberg O'Connor T, Zhao Y et al (2020) The role of cell geometry when selecting tab or surface cooling to minimise cell degradation. *eTransportation* 5:100073. <https://doi.org/10.1016/j.etrans.2020.100073>
 123. Howes JC, Levett DB, Wilson ST, Marsala J, Saums DL (2008) Cooling of an IGBT drive system with vaporizable dielectric fluid (VDF). In: 2008 Twenty-fourth annual IEEE semiconductor thermal measurement and management symposium, 2008. IEEE, pp 9–15
 124. Jiang Y, Zheng Q, Dong P et al (2015) Conjugate heat transfer analysis of leading edge and downstream mist–air film cooling on turbine vane. *Int J Heat Mass Transf* 90:613–626. <https://doi.org/10.1016/j.ijheatmasstransfer.2015.07.005>
 125. Yang Y, Yang L, Du X, Yang Y (2019) Pre-cooling of air by water spray evaporation to improve thermal performance of lithium battery pack. *Appl Therm Eng* 163:114401. <https://doi.org/10.1016/j.applthermaleng.2019.114401>
 126. Saw LH, Poon HM, Thiam HS et al (2018) Novel thermal management system using mist cooling for lithium-ion battery packs. *Appl Energy* 223:146–158. <https://doi.org/10.1016/j.apenergy.2018.04.042>
 127. Kumari N, Bahadur V, Hodes M et al (2010) Analysis of evaporating mist flow for enhanced convective heat transfer. *Int J Heat Mass Transf* 53:3346–3356. <https://doi.org/10.1016/j.ijheatmasstransfer.2010.02.027>

Publisher's Note Springer Nature remains neutral with regard to jurisdictional claims in published maps and institutional affiliations.

Springer Nature or its licensor (e.g. a society or other partner) holds exclusive rights to this article under a publishing agreement with the author(s) or other rightsholder(s); author self-archiving of the accepted manuscript version of this article is solely governed by the terms of such publishing agreement and applicable law.